Vegetation Representation Influences Projected Streamflow Changes in the Colorado River Basin

WILLIAM RYAN CURRIER,[a,b] ANDREW W. WOOD,[b] NAOKI MIZUKAMI,[b] BART NIJSSEN,[c] JOSEPH J. HAMMAN,[d] AND ETHAN D. GUTMANN[b]

[a] *National Oceanic and Atmospheric Administration/Earth System Research Laboratories/Physical Sciences Laboratory, Boulder, Colorado*
[b] *Research Applications Laboratory, National Center for Atmospheric Research, Boulder, Colorado*
[c] *Department of Civil and Environmental Engineering, University of Washington, Seattle, Washington*
[d] *Earthmover, New York, New York*

(Manuscript received 19 August 2022, in final form 25 April 2023, accepted 27 April 2023)

ABSTRACT: Vegetation parameters for the Variable Infiltration Capacity (VIC) hydrologic model were recently updated using observations from the Moderate Resolution Imaging Spectroradiometer (MODIS). Previous work showed that these MODIS-based parameters improved VIC evapotranspiration simulations when compared to eddy covariance observations. Due to the importance of evapotranspiration within the Colorado River basin, this study provided a basin-by-basin calibration of VIC soil parameters with updated MODIS-based vegetation parameters to improve streamflow simulations. Interestingly, while both configurations had similar historic streamflow performance, end-of-century hydrologic projections, driven by 29 downscaled global climate models under the RCP8.5 emissions scenario, differed between the two configurations. The calibrated MODIS-based configuration had an ensemble mean that simulated little change in end-of-century annual streamflow volume (+0.4%) at Lees Ferry, Arizona, relative to the historical period (1960–2005). In contrast, the previous VIC configuration, which is used to inform decisions about future water resources in the Colorado River basin, projected an 11.7% decrease in annual streamflow. Both VIC configurations simulated similar amounts of evapotranspiration in the historical period. However, the MODIS-based VIC configuration did not show as much of an increase in evapotranspiration by the end of the century, primarily within the upper basin's forested areas. Differences in evapotranspiration projections were the result of the MODIS-based vegetation parameters having lower leaf area index values and less forested area compared to previous vegetation estimates used in recent Colorado River basin hydrologic projections. These results highlight the need to accurately characterize vegetation and better constrain climate sensitivities in hydrologic models.

SIGNIFICANCE STATEMENT: Understanding systemic changes in annual Colorado River basin flows is critical for managing long-term reservoir levels. Single-digit percentage decreases have the potential to degrade the regions' water supply, hydropower generation, and environmental concerns. Hydrology projections under climate change have largely been based on simulations from the Variable Infiltration Capacity model. Updating the model's vegetation representation based on updated satellite information highlighted the sensitivity of the hydrologic projections to the models' vegetation representation primarily within forested areas. This updated model did not increase in evapotranspiration by the end of the century as much as previous simulations. This increased the mean and ensemble spread of the projected streamflow changes, emphasizing the need to properly characterize the hydrologic model's vegetation parameters and better constrain model climate sensitivity.

KEYWORDS: Forest canopy; Water resources; Climate change; Evapotranspiration; Hydrology; Hydrologic models

1. Introduction

Regional hydrologic changes in a future climate are commonly estimated using a system of models, termed the impact modeling chain (Bosshard et al. 2013). The impact modeling chain uses various representative concentration pathways (RCPs), global climate models (GCMs), downscaling methods, and hydrologic models to estimate a spread of future projections in streamflow, snow water equivalent (SWE), and evapotranspiration (ET). The choices in hydrologic model structure (Addor et al. 2014; Vano et al. 2012; Vaze et al. 2010) and parameterization (Bastola et al. 2011; Mendoza et al. 2015; Merz et al. 2011) have been identified as important decisions when evaluating the hydrologic change signal, especially in water limited environments such as the Colorado River basin, where evapotranspiration is the dominant process within the water balance (Chegwidden et al. 2019).

Christensen et al. (2004) and Christensen and Lettenmaier (2007) pioneered the top-down, impact modeling chain approach

Denotes content that is immediately available upon publication as open access.

Supplemental information related to this paper is available at the Journals Online website: https://doi.org/10.1175/JHM-D-22-0143.s1.

Corresponding author: William Ryan Currier, william.r.currier@noaa.gov

DOI: 10.1175/JHM-D-22-0143.1

to assess hydrologic changes in the Colorado River basin using the Variable Infiltration Capacity (VIC) hydrologic model (Hamman et al. 2018; Liang et al. 1994). They showed that by the end of the twenty-first century (2070–99), annual streamflow volume was projected to decrease by 8%–17% relative to the historical period (1950–99). Since these early studies, subsequent reports and journal articles have also used VIC with different emission scenarios, GCMs, downscaling methods, and different versions of VIC (Gao et al. 2011; Harding et al. 2012; U.S. Bureau of Reclamation 2011a; Brekke et al. 2014; Vano et al. 2020).

A previous journal article (Vano et al. 2014) and the most recent state of the science report on the climate and hydrology in the Colorado River basin (Lukas and Payton 2020) worked to reconcile and summarize studies since Christensen et al. (2004). These summaries also include studies that use hydrologic models other than VIC (e.g., Alder and Hostetler 2019; Ficklin et al. 2013), or adopt alternative approaches for impact modeling (Lehner et al. 2019; McCabe and Wolock 2007; Milly and Dunne 2020; Seager et al. 2007, 2013; Udall and Overpeck 2017). Most of these studies showed a projected ensemble mean that had annual streamflow volume decrease by the mid-twenty-first century with a range from −10% to −40%.

Some generalized and notable differences across the range of efforts are that in the upper Colorado River basin, the Coupled Model Intercomparison Project phase 5 (CMIP5) collection of GCMs showed a multimodel mean increase in precipitation compared to the previous CMIP (CMIP3; Brekke et al. 2013). In addition, studies that did not incorporate downscaling and used output directly from the GCMs (Milly and Dunne 2020; Seager et al. 2013), or studies that did not account for projected precipitation changes (Udall and Overpeck 2017), found stronger decreases in annual streamflow. The relatively coarse representation of topography in GCMs led to a smaller or nonexistent snowpack, increased evapotranspiration, and decreased streamflow by the end of the century (Lukas and Payton 2020; Milly and Dunne 2020). Furthermore, assuming no change in precipitation, due to disagreement in GCM precipitation projections, streamflow projections show a decrease of approximately 6.5% $°C^{-1}$ of warming (Udall and Overpeck 2017). Under the RCP8.5 emissions scenario, this sensitivity leads to a decrease of −35% by the end of the century (Lukas and Payton 2020; Udall and Overpeck 2017). Therefore, projected increases in precipitation, as shown by the CMIP5 multimodel ensemble mean, offsets losses due to warming.

Since the study by Christensen et al. (2004), gridded meteorological datasets have become available at a higher resolution, and so too have the parameters used for the VIC hydrologic model (Bohn and Vivoni 2019; Livneh et al. 2013). Simultaneously, the VIC code has changed (Bohn and Vivoni 2019; Brekke et al. 2014; Hamman et al. 2018), and new vegetation parameters have become available based on advancements in remotely sensed vegetation characteristics (Bohn and Vivoni 2016, 2019).

New vegetation parameters include changes to the leaf area index and have introduced fractional canopy areas within VIC vegetation tiles. These changes have led to more physically realistic evapotranspiration simulations by including soil evaporation in addition to transpiration within VIC's vegetation tiles. Furthermore, these changes showed improved simulations of total evapotranspiration compared to eddy covariance towers within the geographic region impacted by the North American monsoon (southwestern United States and western Mexico) (Bohn and Vivoni 2016). The importance of evapotranspiration in water limited regions like the Colorado River basin along with the prevalent use of VIC in Colorado River basin climate change studies motivated a reassessment of future hydrologic projections with this new version of the VIC model and its parameters. The VIC model had not been systematically recalibrated since the 2004 study, and updates to the model, its forcings, and to unregulated streamflow datasets in the Colorado River basin compel a model recalibration effort as part of this reassessment.

Here, we incorporated updated vegetation parameters (Bohn and Vivoni 2016, 2019) and recalibrated VIC soil parameters within the Colorado River basin using streamflow observations and the most recent version of the VIC model, VIC 5.1.0 rc2 (Hamman et al. 2018). The recalibrated VIC model with the updated vegetation dataset was then used to evaluate how the change in vegetation datasets, code, and soil parameters affect hydrologic projections using 29 GCMs under the RCP8.5 emissions scenario with the localized constructed analog (LOCA) downscaling technique (Pierce et al. 2014). A single emissions scenario (RCP8.5) was chosen over other emissions scenario to focus on how the changes to the VIC configurations affect the hydrologic projections and to stress test the sensitivity of the Colorado River basin by representing a high emissions, high-risk scenario, with the largest changes in temperature and hydrologic fluxes (Lukas and Payton 2020; Vano et al. 2020). In doing so, we focus on how the end-of-century hydrologic projections change compared to a VIC configuration used in three recent reports (Lukas and Payton 2020; U.S. Bureau of Reclamation 2021; Vano et al. 2020). This paper specifically focuses on changes in simulated evapotranspiration, routed streamflow, and SWE.

2. Data and methods

a. Study domain

Streamflow in the Colorado River basin (Fig. 1) is largely driven by snowmelt (~70%) (Li et al. 2017), with about 50% of the annual precipitation in the form of snow (Rumsey et al. 2015). Estimated losses due to evapotranspiration can account for 75%–98% (5% and 95% quantiles) of annual precipitation depending on the location, with the mountains in the upper Colorado River basin having the highest runoff ratios. The Colorado River basin as a whole has 74 km^3 (60 million acre feet) of total reservoir storage. These 74 km^3 equal around 4 times the annual streamflow volume that passes through Lees Ferry, Arizona (AZ), the legal compact point separating the upper and lower portions of the basin. The large reservoir storage capacity provides a buffer to shield stakeholders against interannual variability in streamflow volumes, but understanding potential systemic changes in annual

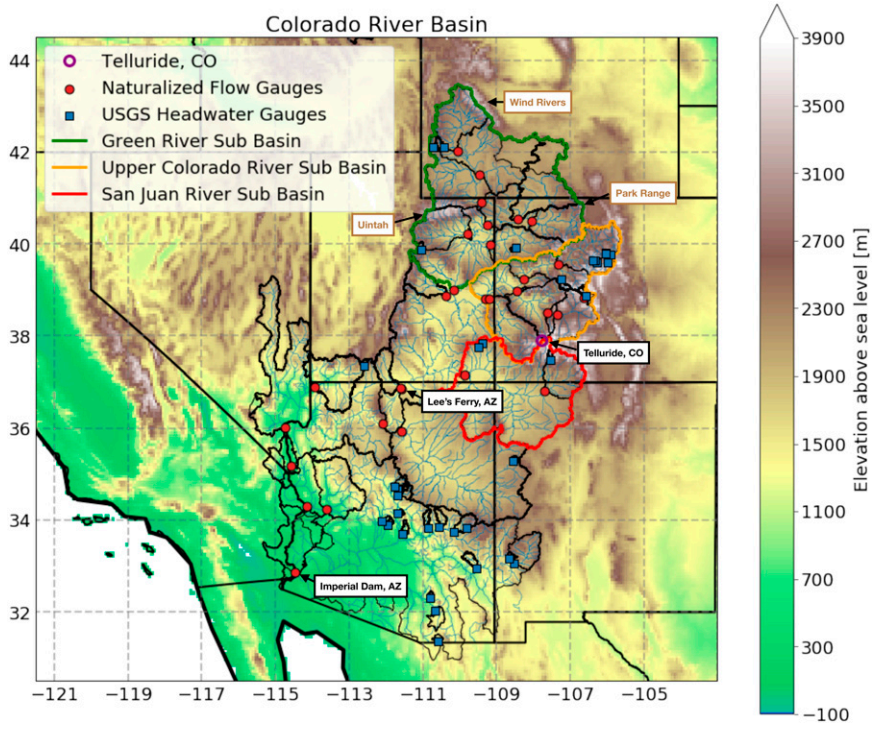

FIG. 1. Colorado River basin in the southwestern United States. Black polygons within the Colorado River basin depict watershed delineations for naturalized flow gauge sites and USGS headwater gauges. The upper Colorado River basin consists of three main watersheds above Lees Ferry, AZ; the Green River; upper Colorado River; and San Juan River subbasins. Each subbasin accounts for 34%, 42%, and 13% of the historic naturalized streamflow at Imperial Dam, respectively. Brown boxes highlight mountain ranges specifically referenced later in the text.

flows is nonetheless critical. Such changes are manifested over the long term in reservoir levels, with even single digit percentage decreases having the potential to degrade the regions' water supply, hydropower generation, and environmental outcomes. Between 2000 and 2019 average naturalized annual flow at Lees Ferry has been 15% of the long-term average (1906–2019) (Lukas and Payton 2020), and total water storage capacity in the Colorado River basin is 40% of capacity. This has led to recent water delivery cutbacks for Arizona, Nevada, and Mexico. Therefore, projected decreases in streamflow would likely lead to further water usage cutbacks. Meanwhile, shifts in the timing of peak streamflow are important for reservoir operations and water users that depend on direct diversion for irrigation, as well as instream flow augmentation pulses to support aquatic habitat.

b. *Historical observations*

1) STREAMFLOW DATA

We used daily streamflow observations from 37 USGS gauges located in the Colorado River basin's headwaters (Table S1 in the online supplemental material). Furthermore, we used naturalized monthly streamflow at 29 additional locations (Table S2), totaling to 66 calibration points for VIC (Fig. 1). In the headwater basins, we selected gauges for calibration based on following criterion: 1) USGS gauges classified as a Hydro-Climatic Data Network 2009 (HCDN-2009) gauge (Falcone 2011; Lins 2012), which excludes notable anthropogenic activity, such as artificial storage and diversions, or any other activity that would significantly alter the natural streamflow, and 2) streamflow record is complete between 1990 and 2009. The streamflow data at all the headwater basins are available in the Catchment Attributes and Meteorology for Large-Sample Studies (CAMELS) dataset (Newman et al. 2014, 2015). At mainstem reservoir locations we used naturalized monthly flow data, which removed the effect of consumptive use, transbasin diversions, and reservoir operations from the streamflow record (Prairie and Callejo 2005). Along the Gila River and its tributaries within the lower Colorado River basin, routed streamflow was only calibrated at a limited number of USGS gauges that were not affected by water withdrawals and storage. Naturalized flow records were not used because of methodological inconsistencies in the consumptive use estimates and loss reports. Additionally, the Gila River joins the mainstream of the Colorado River downstream of all significant storage reservoirs in the basin (U.S. Bureau of Reclamation 2012, 2011b).

2) METEOROLOGICAL DATA

Livneh et al. (2013) 1/16° gridded daily meteorological data were used for model calibration. Livneh et al. (2013) data were used in the calibration of VIC to be consistent with

TABLE 1. Major differences between the two sets of VIC model parameters used in this paper.

	$VIC_{LOCA\text{-}L13}$	VIC_{BV}
Vegetation source	Advanced Very High Resolution Radiometer (AVHRR) imagery and University of Maryland classification scheme	Moderate Resolution Imaging Spectroradiometer (MODIS) MOD12Q.005 product with the IGBP classification scheme
LAI: Leaf area index	Spatial: Constant between land cover types Temporal: Varies from month to month for some land cover types	Spatial: Varies from grid cell to grid cell Temporal: Varies from month to month
fVeg: Fractional area of the vegetation within a VIC tile	Covers 100% of the vegetation tile. Does not vary temporally.	Covers up to 100% of the vegetation tile but often less. Varies from month to month.
Albedo	Spatial: Constant between land cover types Temporal: Varies from month to month for some land cover types	Spatial: Varies from grid cell to grid cell Temporal: Varies from month to month
Soil parameters	Calibrated in Livneh et al. (2013). See text for more details.	Calibrated in this paper using the updated vegetation parameters from Bohn and Vivoni (2019) against naturalized and unregulated stream gauges. See text for more details.

LOCA's training data (section 2c). The Livneh et al. (2013) data included daily precipitation, minimum and maximum daily air temperature, and daily wind speeds. More details on the Livneh et al. (2013) data are provided in the supplemental material (Text S1) (Livneh et al. 2013; Daly et al. 2008). Daily precipitation, temperature, and wind speeds were temporally disaggregated to 3-h intervals using MetSim (Bennett et al. 2020). MetSim was also used to estimate 3-h short- and longwave radiation, humidity, and air pressure. MetSim is a Python-based wrapper for the MTCLIM algorithm (Bohn et al. 2013), which was incorporated as an internal routine in VIC prior to VIC version 5.

c. *Global climate models and downscaled meteorological projections*

We used 29 GCMs from CMIP5 (Table S4). The GCMs were bias corrected and downscaled using LOCA (Pierce et al. 2014). LOCA data were provided at a 1/16° grid spacing (~7 km × 7 km) and provided daily estimates of precipitation and temperature. LOCA used a frequency-dependent bias correction and also notably preserves the predicted precipitation and temperature change signal from the GCM (Pierce et al. 2015), rather than allowing it to be altered in the downscaling process. LOCA uses spatial analogs to relate regional patterns of precipitation or temperature to a downscaled local representation. A collection of analogs is identified for a given region by finding the best matches between the bias corrected GCM climate and coarsened observations. The regions are defined based on the autocorrelation in observed climate, so that only local grid cells identified as related to a given point are used in the matching. From this collection, a small region immediately adjacent to the grid cell to be downscaled is used to select a single "best" analog date, and the high-resolution data from the observations are used at that point. LOCA is trained on the Livneh et al. (2013) observational dataset.

LOCA data have been used in the Fourth National Climate Assessment (USGCRP 2018) and the 2021 SECURE (Science and Engineering to Comprehensively Understand and Responsibly Enhance) Water Act report (U.S. Bureau of Reclamation 2021). Furthermore, the LOCA climate and hydrology datasets were featured in the most recent state of the science report for the Colorado River basin (Lukas and Payton 2020) and in a recent Bureau of Reclamation report (Vano et al. 2020). We used 6 more GCMs from the LOCA ensemble than Vano et al. (2020), which selected downscaled GCMs based on availability for both LOCA and the bias corrected and spatial disaggregation method (BCSD) (Wood et al. 2004). Here, we only focus on using the LOCA downscaled data and therefore the results presented herein do not match exactly with those from Vano et al. (2020).

d. *Hydrologic model datasets*

We used two sets of VIC model parameters (Table 1). Each set had different vegetation and soil parameters. Both sets of VIC model simulations were forced using the same historical meteorological data [section 2b(2)] and the same number of GCMs, downscaled using LOCA (section 2c).

One set contains vegetation and soil parameters primarily from Livneh et al. (2013), and are at a finer-resolution than those developed by Maurer et al. (2002). The hydrologic projections that used this VIC configuration with LOCA climate projections have been featured in three recent reports (Lukas and Payton 2020; U.S. Bureau of Reclamation 2021; Vano et al. 2020). These hydrologic projections used VIC version 4.2.c. From here on this VIC configuration is referred to as $VIC_{LOCA\text{-}L13}$. Livneh et al. (2013) land cover types were based on Advanced Very High Resolution Radiometer (AVHRR) imagery acquired in the early 1990s and a University of Maryland classification scheme (Hansen et al. 2000) (Fig. 2). The $VIC_{LOCA\text{-}L13}$ runs used leaf area index (LAI)

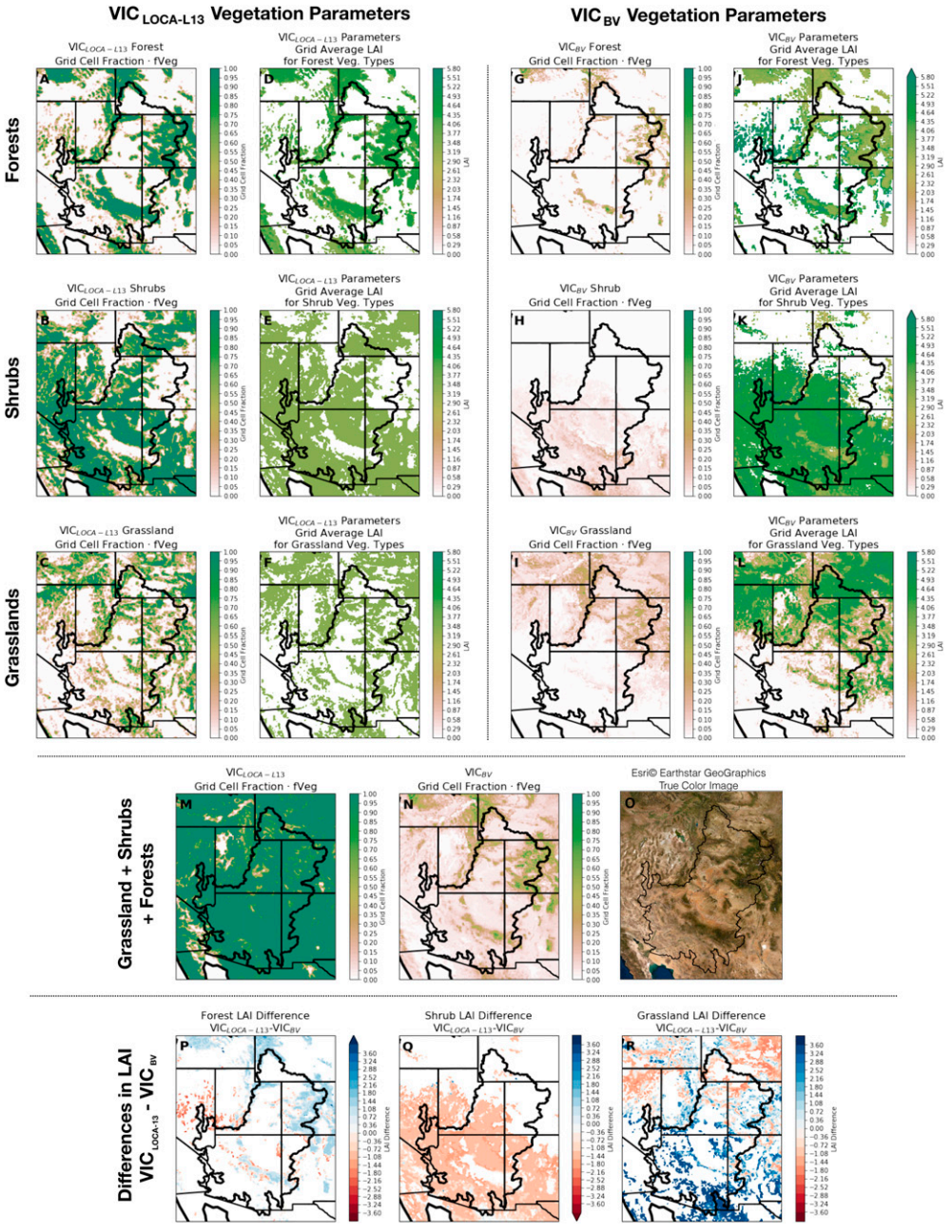

FIG. 2. (a)–(c) $VIC_{LOCA\text{-}L13}$ spatial distribution of different land cover types. The gridcell fraction multiplied by fVeg for different land cover types summed among forest, shrubs, and grassland land cover types. Gridcell fraction is the fraction of the 1/16° grid cell covered by a land cover type, or the fractional area of a VIC vegetation tile; fVeg is the fractional area of the vegetation within a tile. In $VIC_{LOCA\text{-}L13}$ this is equal to 1. Forests were defined as land cover types with an overstory. Shrubs combined open and closed shrublands. (g)–(i) As in (a)–(c), but for VIC_{BV}. In VIC_{BV}, fVeg is less than or equal to 1. (d)–(f),(j)–(l) The leaf area index for different land cover types. The LAI shown here was a weighted average between different land cover types, where the gridcell fractions were the weights. (m),(n) As in (a)–(c) and (g)–(i), but all land cover types were combined to show the spatial distribution of vegetation and the fractional area of each land cover type in $VIC_{LOCA\text{-}L13}$ and VIC_{BV} grid cells. (o) A true color satellite image from ESRI for comparison of vegetated areas in (m) and (n). (p)–(r) The difference in LAI between $VIC_{LOCA\text{-}L13}$ and VIC_{BV} where they overlapped. The fVeg and LAI varied based on month, therefore the average of LAI and fVeg during summer (JJA) was used because that is when evapotranspiration rates were highest.

values referenced from the vegetation library used in earlier studies (Maurer et al. 2002; see supplemental material). These LAI values were based on literature values for individual vegetation types instead of LAI values specified in the parameter file for each grid cell. This makes the LAI decision in $VIC_{LOCA\text{-}L13}$ different from hydrologic model simulations shown in Livneh et al. (2013). Albedos for each land cover type were derived from the literature and were therefore spatially invariant between different land cover types. Furthermore, each land cover type was assumed to cover the entire tile, or fraction of the grid cell that the land cover type covered. Therefore, fVeg equaled 1, as fVeg did not exist in this earlier version (Figs. 2a–c,m).

Soil properties used in $VIC_{LOCA\text{-}L13}$, such as the bulk density, soil particle density, saturated hydraulic conductivity, and the wilting/critical points were derived from the National Cooperative Soil Survey's State Soil Geographic Dataset (STATSGO) (Livneh et al. 2013; Miller and White 1998). The VIC infiltration and baseflow parameters were initially calibrated using VIC version 4.0.3 in Maurer et al. (2002) and then updated using VIC version 4.0.6 in climate change and forecasting applications (Christensen et al. 2004; Christensen and Lettenmaier 2007; Wood and Lettenmaier 2006) using a 1/8° dataset to a subset of streamflow gauges in the Colorado River basin. The updated 1/16° dataset in Livneh et al. (2013) used a Monte Carlo search to calibrate the infiltration curve parameter b, the maximum velocity of baseflow parameter Ds_{max}, and the depth of the bottom soil layer D_3 to match the runoff ratios in Maurer et al. (2002).

Recently, new vegetation parameters were derived using Moderate Resolution Imaging Spectroradiometer (MODIS) observations from the 2001–13 period (Bohn and Vivoni 2019). These new vegetation parameters used MODIS observations to derive fractional vegetation within VIC vegetation tiles, which improved estimated evapotranspiration within the North American monsoon area against Ameriflux observations (Bohn and Vivoni 2016, 2019). From Bohn and Vivoni (2019), we selected the land cover classification from MODIS that used the mode of the vegetation classes from 13 annual classification maps (2001–13) (MOD_IGBP.mode). MOD_IGBP.mode was derived from the MOD12Q.005 product that used the International Geosphere–Biosphere Programme (IGBP) classification scheme. We selected the MOD_IGBP.mode over the National Land Cover Dataset (NLCD) maps that were also generated in Bohn and Vivoni (2019) as the mode provided the most common representation of vegetation over the 2001–13 period (NLCD was only derived for specific years) and MODIS based parameters were used in the Bohn and Vivoni (2016) study. We tested the MODIS and NLCD products and found similar streamflow performance between them. In addition to the introduction of the fractional vegetation within VIC vegetation tiles, the new MODIS parameters from Bohn and Vivoni (2019) updated the seasonal cycle of albedo and LAI to vary monthly.

The new MODIS derived VIC vegetation parameters from Bohn and Vivoni (2019) differ from $VIC_{LOCA\text{-}L13}$ in three ways. First, the MODIS derived parameters from Bohn and Vivoni (2019) have LAI and albedo values that vary spatially, even between areas with the same land cover type. Second, MODIS derived LAI values are now generally lower in forested and grassland areas (Figs. 2p–r). And third, in the MODIS derived parameters, the fVeg parameter is now spatially and temporally varying, which allows for bare soil evaporation to occur in addition to transpiration within a vegetation tile (Bohn and Vivoni 2016) (Figs. 2m,n).

The MODIS derived VIC vegetation parameters from Bohn and Vivoni (2019) were combined with a new streamflow calibration (section 2d) across the Colorado River basin, and the resulting parameter set is referred to as VIC_{BV} throughout the remainder of the paper. Soil parameters for $VIC_{LOCA\text{-}L13}$ and VIC_{BV} were identical prior to model calibration. VIC_{BV} contains the soil calibration (section 2e) performed in this paper.

In both $VIC_{LOCA\text{-}L13}$ and VIC_{BV}, the simulated total runoff (surface and baseflow) was used to drive the mizuRoute streamflow routing model (Mizukami et al. 2016). Streamflow was routed at a daily time step through the reach-defined (rather than grid-based) river network defined in the United States Geological Survey (USGS) Geospatial Fabric dataset (Viger and Bock 2014). MizuRoute used the impulse response function–unit hydrograph procedure, which mimicked the Lohmann et al. (1996) routing model.

e. Calibration

The calibration was done using VIC 5.1.0 rc2 with the MODIS derived VIC vegetation parameters from Bohn and Vivoni (2019). Prior to calibration the soil parameters were identical to $VIC_{LOCA\text{-}L13}$ and only the vegetation parameters were different. The calibration sought to adjust the soil parameters (Table 2) to minimize errors in simulating daily and monthly streamflow (depending on availability). The dynamically dimensioned search (DDS) algorithm (Tolson and Shoemaker 2007) within the program Ostrich (Matott et al. 2013) was used to adjust the soil parameters. The calibration was performed for individual basins, starting with the headwater USGS gauges and then followed by another USGS gauge, or a naturalized flow point, downstream from one another. Contributing VIC grid cells were identified, and the soil parameters were adjusted to optimize the Kling–Gupta efficiency (KGE) (Gupta et al. 2009) using daily values for the headwater gauges and monthly values for the naturalized flow points. The KGE combines the correlation, bias, and ratio of variances, with a value of 1 indicating a perfect model simulation. The maximum KGE achieved after each iteration within DDS for each gauge is shown in the supplemental material (Figs. S1 and S2). DDS was run until the KGE appeared to have reached a maximum value. Once an upstream basin was calibrated, those soil parameters were held constant and the next basin downstream was calibrated using the remaining contributing grid cells. Each iteration during calibration was initialized with a 10-yr spinup period (water year 1991–2001). The KGE was optimized for water years 2001–10. The final soil parameters before and after calibration are shown in the supplemental material (Fig. S3).

3. Results

a. Model calibration

The uncalibrated VIC_{BV} model that contained the new vegetation parameters produced a median KGE value of 0.59

TABLE 2. Calibration parameters and the range and initial value within the model parameter values.

Soil parameter name	Definition	Search range (initial value)
b (—)	Variable infiltration curve parameter	0.001–0.4 (0.2)
Ds_{max} (mm day^{-1})	Maximum velocity of baseflow	0.001–30.0 (15)
Ds (fraction)	Fraction of Ds_{max} where nonlinear baseflow begins	0.001–1.0 (0.001)
Ws (fraction)	Fraction of maximum soil moisture where nonlinear baseflow occurs	0.5–1.0 (0.9)
Soil depth 1–3 (m)	Thickness of each soil layer	0.1–0.5 (0.5) 0.5–1.5 (1) 0.5–3.0 (2)
Root fraction multiplier (—)	Adjusted the bottom soil layers root fraction with a multiplier and normalized the remaining soil layers root fraction so that the three soil layers root fraction summed to 1	0.4–6.0 (1)

and a standard deviation of 1.66 across the 29 naturalized streamflow points between 1960 and 2013. After the soil parameters were calibrated, the VIC_{BV} model resulted in a median KGE value of 0.82 and a standard deviation of 0.49 at the 29 naturalized flow points between 1960 and 2013 (Fig. 3). The $VIC_{LOCA\text{-}L13}$ configuration produced a median KGE value of 0.75 and a standard deviation among KGE values of 0.47 across the 29 naturalized flow points between 1960 and 2013. At mainstem locations (Fig. 1) such as the Green River at Green River, Utah (UT); the Colorado River near Cisco, UT; San Juan River near Bluff, UT; Lees Ferry, AZ; and the Colorado River above Imperial Dam, AZ, VIC_{BV} resulted in KGE values of 0.87, 0.9, 0.92, 0.83, and 0.85, respectively. $VIC_{LOCA\text{-}L13}$ resulted in KGE values of 0.84, 0.9, 0.91, 0.76, and 0.82, respectively (Fig. 4).

Across the headwater USGS gauges, the calibration did not result in a notable improvement in streamflow simulations compared to the uncalibrated VIC_{BV}. The median KGE values based on monthly streamflow values before the calibration was 0.16 and after calibration it was 0.17 with a reduction in the standard deviation of 0.1 (3.18 from 3.28). At headwater locations, VIC_{BV} performed worse than $VIC_{LOCA\text{-}L13}$, most notably in the lower Colorado River basin. $VIC_{LOCA\text{-}L13}$ had a 0.3 median KGE (1.5 standard deviation). The VIC_{BV} model configuration produced better or comparable performance to $VIC_{LOCA\text{-}L13}$ configuration in some locations, but performed worse in other areas (Fig. 3).

In general, the VIC_{BV} configuration improved the timing of high streamflow values from year to year (Fig. 4) due to increased snow ablation rates in forested areas. Increased snow ablation rates were the result of less radiation attenuation by the canopy from the introduction of a fractional canopy area and generally lower LAI values (Fig. 2). In summary, $VIC_{LOCA\text{-}L13}$ showed better streamflow performance in some locations while VIC_{BV} showed better performance at other locations making neither parameter dataset comprehensively better than the other.

b. *Hydrologic projections from different VIC configurations*

1) ROUTED STREAMFLOW PROJECTIONS

(i) Changes in annual streamflow volume

The Colorado River basin contains a significant amount of reservoir storage (section 2a), making projected changes in

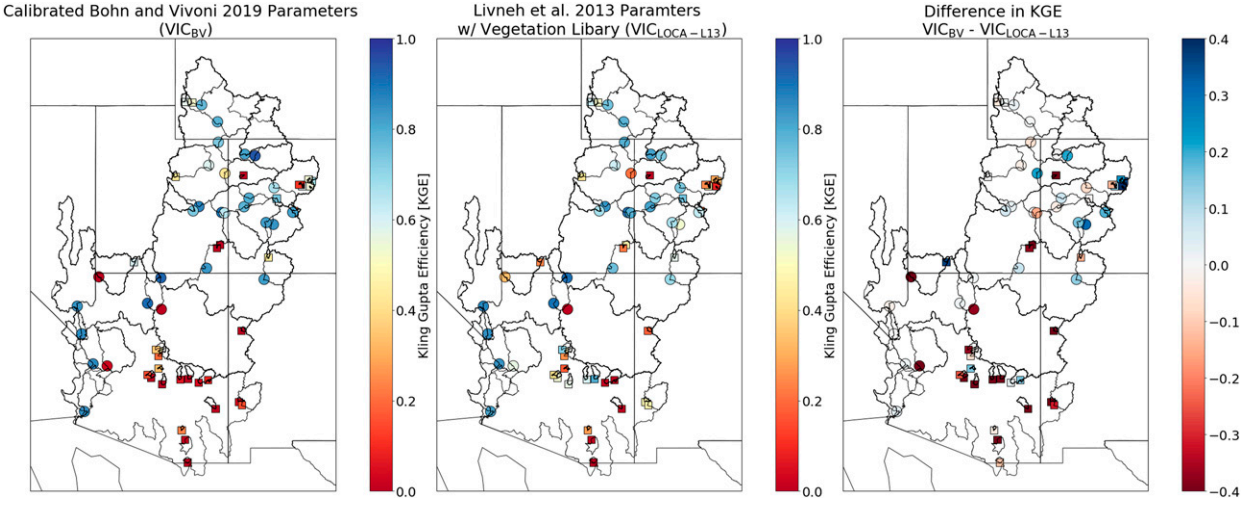

FIG. 3. Kling–Gupta efficiency (KGE) values from VIC_{BV} and $VIC_{LOCA\text{-}L13}$ at the 66 calibration points. The 29 naturalized streamflow values are shown in circles. The 37 USGS headwater water stream gauges are shown with squares. For the 29 naturalized streamflow sites, the KGE was computed between 1960 and 2013. For the 37 USGS headwater stream gauges, the KGE was calculated from 1960, or the beginning of the observational period, until 2013.

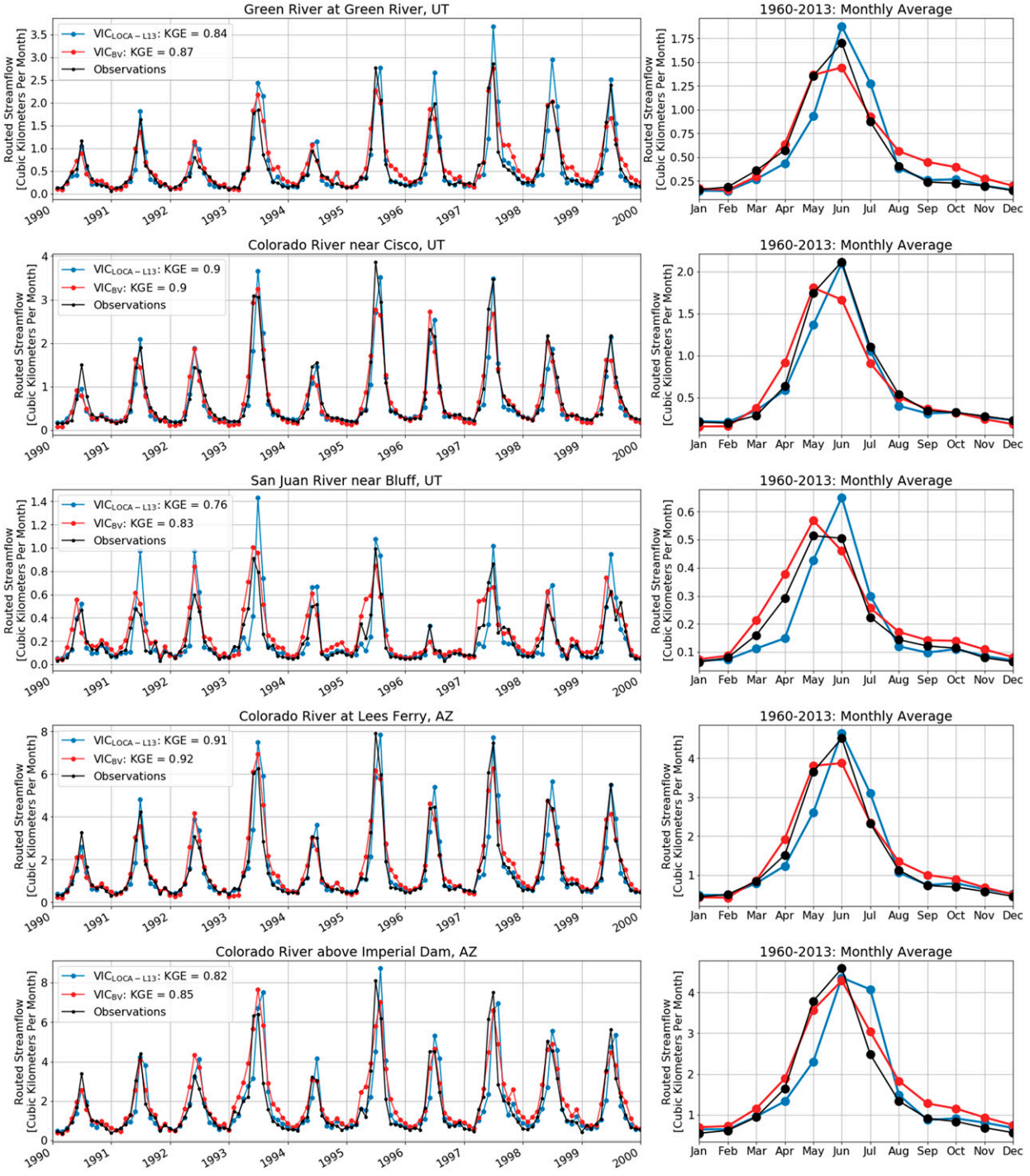

FIG. 4. Routed VIC streamflow from the Livneh et al. (2013) VIC parameters using the vegetation library (blue) and using the Bohn and Vivoni (2019) MODIS-based vegetation parameters after calibration at four mainstem locations in the Colorado River basin. KGE metrics are calculated from 1960 to 2013. Monthly average flows are calculated from 1960 to 2013.

long-term annual streamflow volume more important than short-term variability for many water users. There were notable differences between the $VIC_{LOCA\text{-}L13}$ and VIC_{BV} configurations in their ensemble mean, end-of-century (2070–99), annual streamflow volume projections (Figs. 5 and 6). At Lees Ferry, AZ, which receives 92% of the streamflow that reaches the Imperial Dam (Lukas and Payton 2020), the $VIC_{LOCA\text{-}L13}$ configuration's ensemble mean resulted in a

11.7% decrease in annual streamflow volume relative to the historical period (1960–2005) while the VIC_{BV} configuration's ensemble mean showed little change in annual streamflow volume relative to the historical period (+0.4%).

Breaking apart the flow at Lees Ferry into different subbasins, the Colorado River and San Juan River projected the most substantial decreases in annual streamflow volume. $VIC_{LOCA\text{-}L13}$'s projected ensemble mean showed a decrease in annual streamflow volume of 15.8% in the Colorado River and a 23.1% decrease in the San Juan River. In contrast, the VIC_{BV} ensemble mean projected a decrease in annual streamflow volume of 8.5% in the Colorado River and a 6.3% decrease in the San Juan River. In the Green River, $VIC_{LOCA\text{-}L13}$'s ensemble mean projected a decrease in annual streamflow volume of 6.7% while VIC_{BV}'s projected ensemble mean showed an increase of 9.7%.

The spread in the LOCA ensemble when run through $VIC_{LOCA\text{-}L13}$ resulted in a narrower range of projected changes in streamflow volume than when the LOCA ensemble was run through VIC_{BV}. For instance, at Lees Ferry, the $VIC_{LOCA\text{-}L13}$ ensemble showed projected changes in annual streamflow volume of as low as −40% and as high as +24% (range: 64%) by the end of the century. Meanwhile, the VIC_{BV} ensemble projected changes in annual streamflow volume of as low as −37% and as high as +61% (range: 98%) by the end of the century relative to historical annual streamflow volumes. This is further discussed in section 4d.

(ii) Changes in timing of peak streamflow

The end-of-century ensemble mean for both $VIC_{LOCA\text{-}L13}$ and VIC_{BV} showed a shift to earlier streamflow (Figs. 5 and 6). For each ensemble member we computed the average streamflow for each day of the year within the end of the century and historical periods for $VIC_{LOCA\text{-}L13}$ and VIC_{BV}. From here, we took the difference in days of peak streamflow timing between the end-of-century and historical time periods across all ensemble members. At Lees Ferry, $VIC_{LOCA\text{-}L13}$ ensemble mean showed a shift in peak streamflow timing of 24 days while the VIC_{BV} ensemble mean shifted by 18 days. Mainstem stream gauges upstream of Lees Ferry, AZ, along the Green River, Colorado River, and the San Juan River showed similar changes in peak streamflow timing along each individual river (Fig. 6, bottom panels). The ensemble spread in $VIC_{LOCA\text{-}L13}$ at Lees Ferry showed a projected shift in earlier peak streamflow from 14 to 57 days while the ensemble spread from VIC_{BV} was a shift of 11–50 days earlier.

2) GRIDDED HYDROLOGIC PROJECTIONS

The ensemble mean of 29 LOCA downscaled GCMs projected a 5.6°C areal average increase in temperature by the end of the century in the upper Colorado River basin compared to the historical period 1960–2005 (Figs. 7c,d). Temperature increases were greatest in both the upper Colorado River basin and Green River subbasin. In addition, the LOCA ensemble mean projected an increase in precipitation of 17 mm (4%) (up to maximum of 15%) with the greatest increases in the Green River subbasin (32 mm, 8%), more specifically in the Uintah and Wind River Mountains, as well as the Park Range in south-central Wyoming and north-central Colorado (Figs. 1 and 7a,b, Table 3).

The greatest differences between $VIC_{LOCA\text{-}L13}$ and VIC_{BV} was in their projected increases of simulated evapotranspiration (Figs. 7f,g, Table 3). During the historical period, $VIC_{LOCA\text{-}L13}$ simulated a 330 mm areal average of evapotranspiration (83% of precipitation) annually over the upper Colorado River basin. By the end of the century, $VIC_{LOCA\text{-}L13}$ simulated an areal average increase of 24 mm. VIC_{BV} simulated less evapotranspiration historically (324 mm) and projected an increase in areal average evapotranspiration of 17 mm across the upper Colorado River basin (Table 3). The greatest differences in evapotranspiration occurred in the seasonal snow zone (defined here as where snow is present 180 days of the year). Within the seasonal snow zone, $VIC_{LOCA\text{-}L13}$ simulated an areal average increase of 121 mm while VIC_{BV} simulated an increase of 65 mm.

In the Green River subbasin, where there was the greatest increase in projected precipitation, the ensemble mean from $VIC_{LOCA\text{-}L13}$ simulated a larger increase in evapotranspiration than VIC_{BV}. Increased projected precipitation and less of an increase in evapotranspiration within VIC_{BV} led to a positive change in runoff for VIC_{BV}. The ensemble mean from $VIC_{LOCA\text{-}L13}$ in the Green River projected a −5% change in runoff while the ensemble mean from VIC_{BV} projected a 7% increase in runoff. In the Colorado River and San Juan subbasins within the upper Colorado River basin, the ensemble mean from $VIC_{LOCA\text{-}L13}$ also projected more of an increase in future evapotranspiration than VIC_{BV}'s ensemble mean. Overall, by the end of the century, $VIC_{LOCA\text{-}L13}$ projected more of an increase in evapotranspiration than VIC_{BV}, which led to further decreases in projected streamflow.

The 5.6°C increase in temperature throughout the upper Colorado River basin led to a decrease in future SWE accumulation. In general, throughout the domain $VIC_{LOCA\text{-}L13}$ simulated higher peak SWE than VIC_{BV}, historically and in the future. Despite differences in projected changes of peak SWE, both VIC configurations showed similar differences in their projected decrease of peak SWE (−74 mm versus −65 mm, Table 3). Within the seasonal snow zone, we found that depending on location, $VIC_{LOCA\text{-}L13}$ or VIC_{BV} simulated greater decreases in peak SWE but on average $VIC_{LOCA\text{-}L13}$ simulated a slightly greater decline in SWE. However, within the seasonal snow zone, differences in the evapotranspiration change signal between $VIC_{LOCA\text{-}L13}$ and VIC_{BV} were substantial (Figs. 7f,g) and more closely connected to the changes in runoff (Figs. 7j,k).

4. Discussion

In the following section, we discuss reasons why $VIC_{LOCA\text{-}L13}$ and VIC_{BV} led to different projections of evapotranspiration and streamflow by the end of the century. We also discuss reasons for the spread in projected changes, compare with previous work, and last, discuss avenues for future work.

a. *Sensitivity of hydrologic variables to changes in vegetation*

To understand how different LAI, fVeg, and albedo parameters affect end-of-century hydrologic projections relative to the

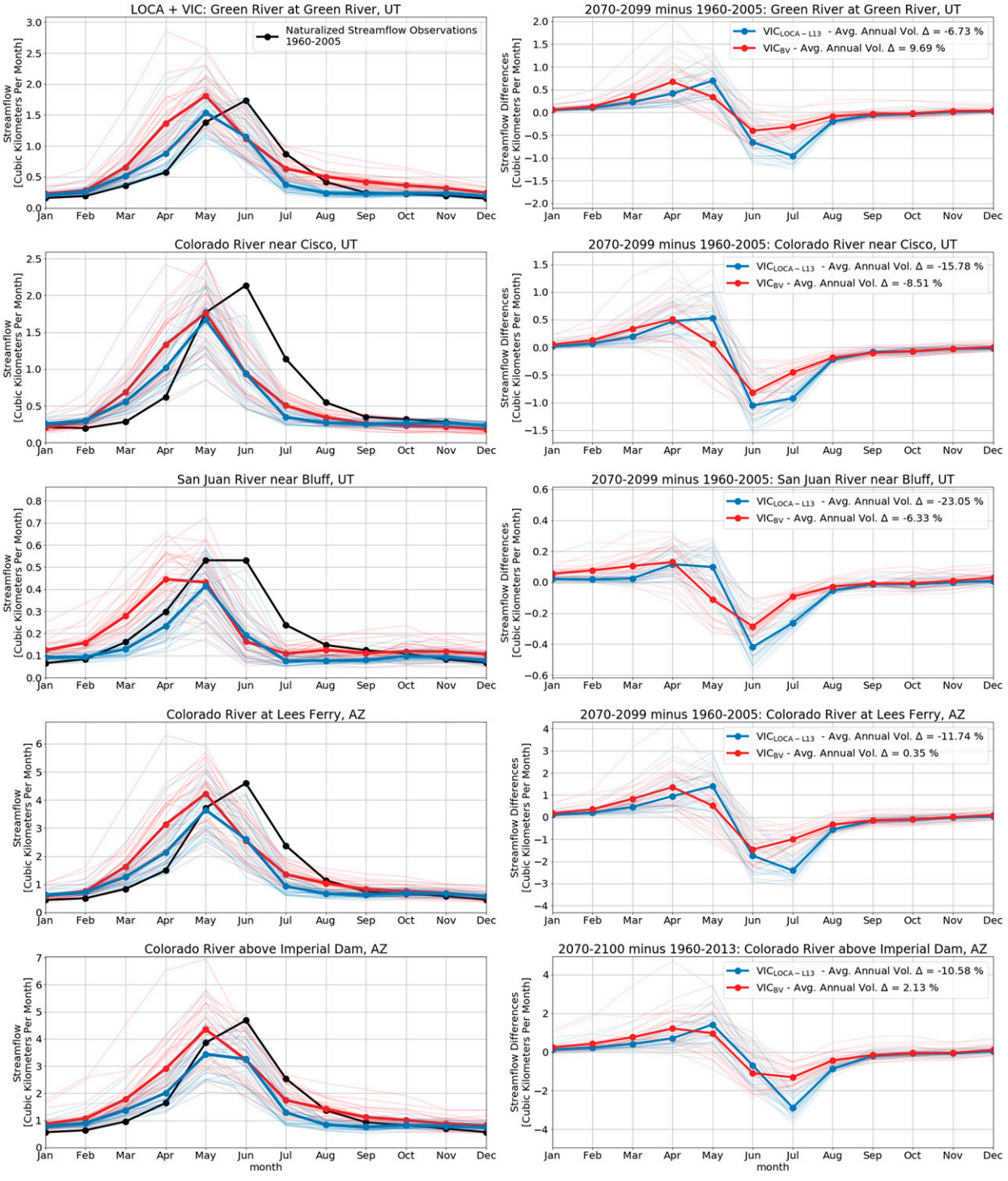

FIG. 5. (left) Projected, end-of-century (2070–99) monthly average routed streamflow ensembles from LOCA and VIC using the calibrated Bohn and Vivoni (2019) parameters (VIC_{BV}) and the Livneh et al. (2013) parameters with the vegetation library ($VIC_{LOCA\text{-}L13}$). (right) End-of-century monthly average streamflow projections minus the 1960–2005 streamflow projections. Thick solid lines show the ensemble mean, while thin lines show the individual ensemble members. The black solid line represents the 1960–2005 historical monthly averaged streamflow.

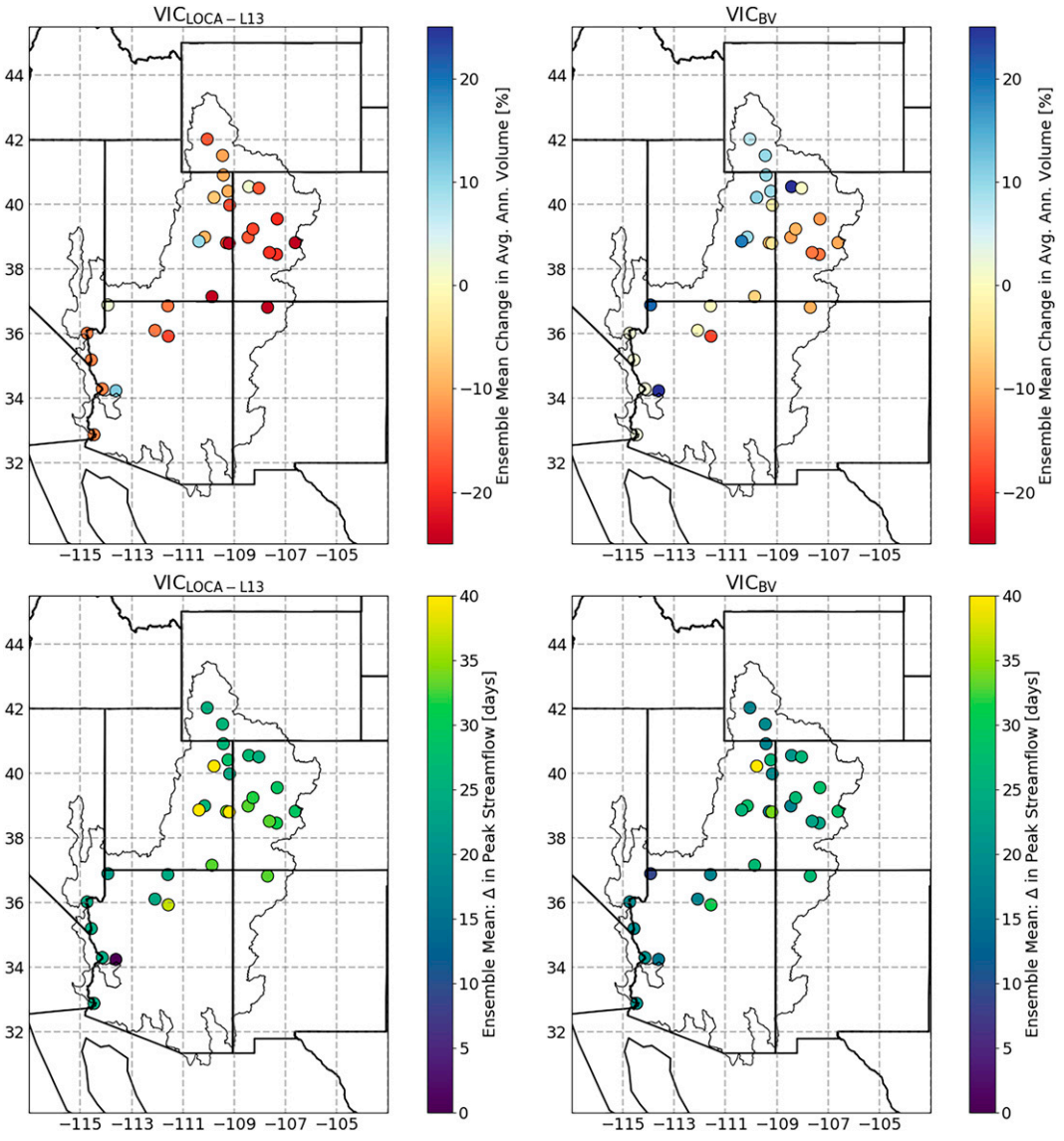

FIG. 6. (top) LOCA and VIC's annual streamflow volume projections (2070–99 minus 1960–2005) at the 29 naturalized stream gauges using the ensemble mean from the calibrated Bohn and Vivoni (2019) parameters (VIC_{BV}) and the Livneh et al. (2013) parameters with the vegetation library ($VIC_{LOCA-L13}$). (bottom) The projected change in peak streamflow timing from the ensemble mean from VIC_{BV} and $VIC_{LOCA-L13}$.

historical period within VIC, we set up a series of experiments within an individual grid cell. Within the main text, the individual grid cell experiment used a grid cell near Telluride, Colorado (CO) (lat: 37.906 25, lon: −107.718 75) (Fig. 1), as this grid cell showed a substantial difference in evapotranspiration, runoff, and SWE between $VIC_{LOCA-L13}$ and VIC_{BV} (Fig. 7). Note the experiment is repeated for different grid cells, which is discussed later and in the supplemental material. For simplicity, these experiments used a single LOCA ensemble member (NorESM1-M) to force VIC with different vegetation parameters. We chose the LOCA downscaled NorESM1-M GCM because its projected change in annual streamflow volume was similar to the ensemble mean. The first experiment changed LAI and fVeg, while the second experiment changed albedo and fVeg. For each experiment, two VIC vegetation scenarios were configured, one with an evergreen needleleaf land cover type while the other with grassland. We changed LAI, albedo, and fVeg while all other vegetation parameters remained consistent with the VIC_{BV} parameter dataset. Each experiment was run through VIC 5.1.0 rc2. LAI was changed from 0.1 to 6.6 in 0.5 increments, fractional vegetation area was changed from 0 to 1 in 0.1 increments, and albedo was changed from 0.05 to 0.5 in increments of 0.05.

The LAI versus fVeg experiment showed that both parameters influenced the hydrologic projections by the end of century (Fig. 8). For instance, as LAI or fVeg increased, so too did the

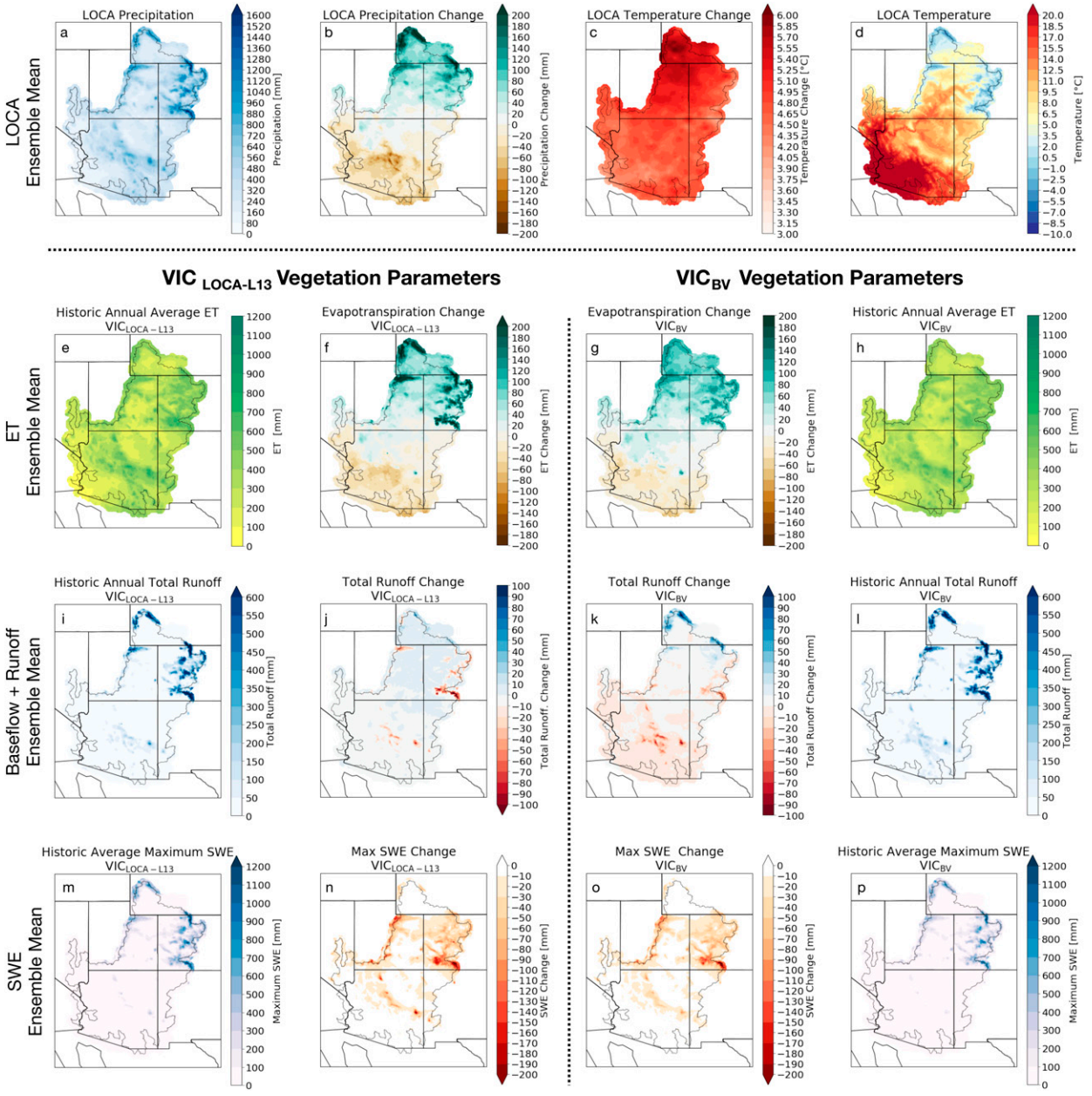

FIG. 7. (first column),(fourth column) Ensemble mean of LOCA downscaled climate data or annual average/maximum simulated fluxes/states (1960–2005) from two different VIC configurations VIC_{BV} and $VIC_{LOCA\text{-}L13}$, respectively. (second column),(third column) Changes in the ensemble mean of downscaled LOCA climate data or changes in annual average/maximum of simulated fluxes/states from the two different VIC configurations (2070–99 minus 1960–2005), respectively.

projected change in total evapotranspiration (Figs. 8a,i). Conversely, as LAI or fVeg increases, projected changes in total runoff decreased (Figs. 8h,p). Furthermore, because the evergreen needleleaf land cover type contains an overstory, projected changes in peak SWE were affected by LAI and fVeg: LAI is embedded in the snow interception parameterization and controls how much shortwave radiation is attenuated (Storck 2000; Andreadis et al. 2009), as well as how much snowfall is intercepted and potentially lost to sublimation.

The evergreen needleleaf land cover type showed a substantially greater change in transpiration (Fig. 8b) than transpiration from grasslands (Fig. 8j), or changes in bare soil evaporation (Figs. 8c,k). In addition, forested areas (Figs. 2a,j) generally corresponded to areas with the greatest differences in projected evapotranspiration change (Figs. 7f,g). The $VIC_{LOCA\text{-}L13}$ parameters have a greater fractional forest area (with fVeg = 1) than VIC_{BV} (Figs. 2a,j) and therefore a larger fraction of the grid cell simulated transpiration, which resulted in the $VIC_{LOCA\text{-}L13}$

TABLE 3. Average annual hydrologic fluxes over the historical period and then averaged (except SWE) over different regions of the upper Colorado River basin (Fig. 1). SWE refences the average annual peak SWE over the historical period and then averaged over the region. Also, the end-of-century change from the historical period (1960–2005) for both $VIC_{LOCA\text{-}L13}$ and VIC_{BV} over the same regions. The seasonal snow zone is defined as locations that have more than 180 days of snow present per year, which are generally located in mountainous areas (Fig. 1).

		Upper Colorado		Green River subbasin		Upper Colorado River subbasin		San Juan River subbasin		Seasonal snow zone	
		Historical	Change	Historical	Change	Historical	Change	Historical	Change	Historical	Change
Precipitation (mm)	LOCA	397	17	400	32	552	14	364	−3	892	43
Evapotranspiration (mm)	$VIC_{LOCA\text{-}L13}$	330	24	332	32	420	36	316	8	514	121
	VIC_{BV}	324	17	323	26	414	25	310	1	462	65
Runoff (mm)	$VIC_{LOCA\text{-}L13}$	67	−8	68	−5	132	−22	48	−11	379	−78
	VIC_{BV}	71	0	75	7	127	−11	53	−3	429	−22
SWE (mm)	$VIC_{LOCA\text{-}L13}$	107	−27	117	−23	195	−49	69	−27	489	−74
	VIC_{BV}	93	−24	106	−21	162	−43	59	−24	417	−65

configuration projecting a greater increase in evapotranspiration by the end of the century than VIC_{BV}. Furthermore, the $VIC_{LOCA\text{-}L13}$ parameters also had higher LAI values than VIC_{BV} for forested and grassland areas (Figs. 2p,r). A higher LAI value corresponded to a greater increase in end-of-century evapotranspiration although changes in LAI were more sensitive for the evergreen needleleaf forest (Figs. 8a,i). This further supported the relationship between forested areas (Figs. 2a,j) and the differences in evapotranspiration between $VIC_{LOCA\text{-}L13}$ and VIC_{BV} (Figs. 7f,g).

This analysis was repeated for nine different historical Köppen–Geiger climate classification regions (Beck et al. 2018) within the Colorado River basin (Figs. S4–S13). Here the analysis also included an open shrubland vegetation classification which showed similar hydrologic change signals due to differences in LAI and fVeg as grassland areas. In general, the most substantial positive relationships between evapotranspiration, LAI, and fVeg, occurred in mountainous forested areas of the seasonal snow zone within the upper basin where the ensemble mean projected increases in precipitation by the end of the century (Fig. 7b). This is consistent with findings from Bennett et al. (2018b), who showed that hydrologic change signals were most sensitive to VIC parameters such as fVeg and LAI in snow-dominated regions. Forested areas generally overlapped with the seasonal snow zone, which is also the area with highest runoff ratios as snowmelt comes at a time when potential evapotranspiration is lower than later in the summer and the snowmelt provides water into saturated soils. Therefore, these areas are not water limited, whereas in other areas of the Colorado River basin the majority of the water is lost to evapotranspiration. In VIC_{BV}, there was substantially less forested area relative to $VIC_{LOCA\text{-}L13}$ (Figs. 2a,g) and therefore despite simulating similar amounts of evapotranspiration historically, $VIC_{LOCA\text{-}L13}$ simulated a greater increase in end-of-century evapotranspiration (Table 3, Figs. 7f,g) as a result of differences in LAI and forest area (Figs. 2 and 8). Evergreen forests produced the greatest changes in evapotranspiration for the same climate and location relative to grassland and shrublands due to deeper roots (Figs. 8a,i).

Last, differences in albedo between $VIC_{LOCA\text{-}L13}$ and VIC_{BV} were relatively small. For instance, across the Colorado River basin differences in evergreen needleleaf albedo during summer (JJA) was on average 0.01 with a maximum difference of 0.03. Meanwhile other land cover types showed similar differences in albedo, generally within 0.1 of each other. Sensitivity to end-of-century changes in annual average evapotranspiration were also relatively small (Fig. S14). For instance, a 0.2 difference in an evergreen needleleaf's albedo resulted in about a 12 mm difference in annual average evapotranspiration by the end of the century.

b. *Hydrologic projections with different VIC versions and effect of soil calibration*

There were several differences between $VIC_{LOCA\text{-}L13}$, which used VIC version 4.2.c, and VIC_{BV}, which used VIC version 5.1.0.rc2. The major changes from VIC 4 to VIC 5 were to improve the computational infrastructure (e.g., improving file

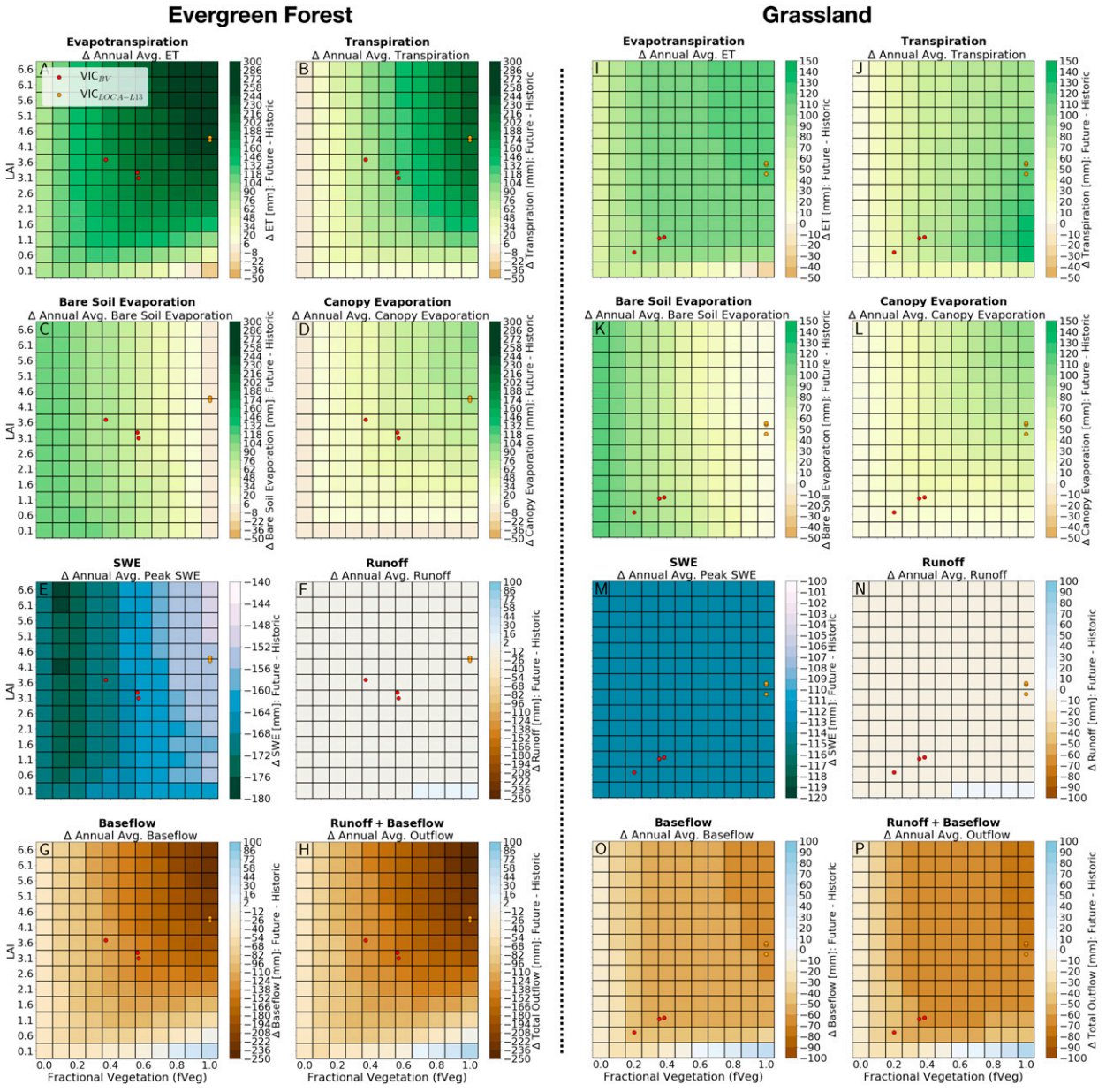

FIG. 8. End-of-century (2070–99) annual average change in hydrologic fluxes and states from historic conditions (1960–2005) for a single grid cell near Telluride, CO, with different vegetation parameters. Note the different color bar scales for evergreen needleleaf and grassland land cover types. Red and orange markers represent the JJA fractional vegetation and LAI values that existed near Telluride, CO, for an evergreen needleleaf and grassland land cover type within VIC_{BV} and $VIC_{LOCA\text{-}L13}$ datasets, respectively.

read and write operations, parallelization, etc.). The changes in the VIC physics code between version 4.2.c and 5.1.0.rc2 were minor and included small changes to the surface emissivity values and a bug fix to appropriately apportion the root fraction to individual soil layers. An additional difference between our VIC_{BV} simulations and $VIC_{LOCA\text{-}L13}$ was that we used a 3-h time step instead of a 1-h time step. More explicit detail and the effect of these changes are discussed in the supplemental material (Text S3; Figs. S15 and S16). To briefly summarize the results here, the changes in the root fraction, surface emissivity, and time step led to an increase in evapotranspiration during the historical period (Fig. S15; red line versus blue line). By the end of the century, these different model decisions led to an increase in annual streamflow volume change relative to the $VIC_{LOCA\text{-}L13}$ configuration but did not change the streamflow timing (Fig. S16; orange line versus blue line). For instance, at Lees Ferry, AZ, the change in annual streamflow volume from the different version of VIC and time step was 5.9% (Fig. S16; orange line versus blue line); however, the change caused by changing the vegetation

parameters alone was 10.9% (Fig. S16; orange line versus purple line). Therefore, the different version of VIC between $VIC_{LOCA\text{-}L13}$ and VIC_{BV} had an influence but was not the predominant reason for differences in the end-of-century streamflow projections.

The change in vegetation parameters prior to soil calibration led to higher snowmelt rates, less evapotranspiration, and an earlier increase in the hydrograph's rising limb (Figs. S15–S17). In contrast, soil calibration did not change the timing of streamflow, but instead increased the total amount of evapotranspiration and decreased the projected change in annual streamflow volume. For instance, prior to soil calibration, the projected change in streamflow volume at Lees Ferry was +5%, while after calibration it was +0.4%. This is consistent with results from Mendoza et al. (2015), who showed that calibration reduces intermodel differences, but that even after calibration, intermodal differences remain in the projected hydrologic change signal. In conclusion, the largest single difference between $VIC_{LOCA\text{-}L13}$ and VIC_{BV} was due to changes to the vegetation parameters, notably LAI and the fractional vegetation.

c. *Interpreting the spread in end-of-century hydrologic projections*

This work showed that the choice in vegetation decisions increased the spread in the ensemble [section 3b(1)]. For instance, at Lees Ferry, the VIC_{BV} ensemble showed projected changes in annual streamflow volume of as low as −37% and as high as 61% by the end of the century relative to historical annual streamflow volumes (1960–2005). This variability was primarily due to projected changes in precipitation from different GCMs (Figs. S18 and S19). Previous work showed that small changes in precipitation can substantially impact future hydrologic projections as a 10% change in precipitation can lead to a 20%–30% change in streamflow (Hoerling et al. 2019; Vano et al. 2012). Furthermore, the temperature and precipitation elasticity for streamflow at Less Ferry, AZ, changed from $-6.5\%\ °C^{-1}$ and $2.3\%\ \%^{-1}$ in $VIC_{LOCA\text{-}13}$ to $-5.8\%\ °C^{-1}$ and $2.6\%\ \%^{-1}$ in VIC_{BV}, respectively. Therefore, VIC_{BV} had less of a decrease in streamflow for an increase in temperature than $VIC_{LOCA\text{-}L13}$ but produced more streamflow with increases in precipitation (Figs. S18 and S19). Additionally, annual streamflow projections that projected an overall decrease in precipitation had similar changes in streamflow between VIC configurations (Table S3). For example, the GCM that projected the greatest decline in streamflow at Lees Ferry, AZ showed a −40% decrease in annual streamflow with $VIC_{LOCA\text{-}L13}$ and −37% with VIC_{BV}. In contrast, projections that showed an increase in streamflow, or less of a decrease in streamflow, showed a greater difference between VIC configurations (Figs. S18 and S19). This is consistent with results from Bennett et al. (2018b) who found that hydrologic projections with VIC are more sensitive to changes in parameters in areas with large precipitation trends.

Last, we note that the spread in annual streamflow volume projections highlights that substantial differences exist based on hydrological model decisions. A more significant uncertainty within the impact modeling chain on projected Colorado River basin annual streamflow volumes is from the GCM precipitation, which in the upper Colorado River basin varied from as low as −12.9% to as a high as +34.6% change. However, the vegetation decisions did increase the sensitivity of the model to precipitation changes (Figs. S18 and S19).

d. *Results in context of recent work*

Recent work has utilized similar vegetation datasets (Bohn and Vivoni 2016, 2019) to look at future hydrologic projections over the Colorado River basin (Whitney et al. 2023) as well as the sensitivity of future hydrologic projections with VIC to different parameter decisions (Bennett et al. 2018b). We found that future hydrologic projections using eight LOCA downscaled CMIP5 GCMs under the RCP8.5 emissions scenario from Whitney et al. (2023) also showed a systematic increase in projected annual streamflow volume relative to projections from $VIC_{LOCA\text{-}L13}$. However, projections and model elasticities to temperature and precipitation changes were more similar to projections in $VIC_{LOCA\text{-}L13}$ than in our VIC_{BV} configuration. We note that there are methodological decisions in Whitney et al. (2023) that differ from those within this paper. For instance, Whitney et al. (2023) had a different calibration strategy, used an older version of VIC (VIC 5.0, which has a different way of apportioning the root fraction), and used time-varying vegetation parameters between 2000 and 2016. For instance, the time-varying vegetation parameters which were used in Whitney et al. (2023) contained up to 10% more fractional forest area and greater LAI values (~0.2) in the future (after 2016) and slightly less fractional forest area in the historical time frame (prior to 2000) (Figs. S20 and S21). This reinforces the idea that hydrologic projections from hydrologic models need to accurately characterize the vegetation in the historical period and in the future to reduce our uncertainty in hydrologic projections. In addition, Bennett et al. (2018b) showed that the choice of the soil parameters can influence the change in runoff and evapotranspiration. We note that the soil parameters from this paper and Whitney et al. (2023) are different and this likely contributed to differences in VIC_{BV} and results in Whitney et al. (2023). Furthermore, this suggests that the interplay between soil parameters and vegetation parameters on the hydrologic change signal may be more complex.

e. *Future work*

There is a clear and long-standing challenge in obtaining spatiotemporal vegetation and soil parameters that combine to accurately simulate evapotranspiration across large domains like the Colorado River basin and therefore further investigation is needed. For instance, while comparisons to satellite imagery (Fig. 2, Fig. S22) look better, and previous work that showed that VIC_{BV} vegetation parameters improved evapotranspiration estimates at eddy covariance sites in the North American monsoon region (Bohn and Vivoni 2016), both $VIC_{LOCA\text{-}L13}$ and VIC_{BV} had similar streamflow performance historically, making it unclear what set of VIC parameters more properly represents runoff processes. Additionally, previous studies have

suggested that LAI values from MODIS are too low (Jensen et al. 2011; Chen et al. 2005; Tian et al. 2004) but as far as we are aware MODIS LAI values have yet to be evaluated over the Colorado River basin. Moreover, future work should focus on improving the algorithm for estimating fractional vegetation from remotely sensed data (Bennett et al. 2018b). Estimates of fractional forest area and LAI from satellite imagery (which allows us to cover longer space and time periods) could be compared to lidar-derived estimates of fractional vegetation area. Further compounding this challenge is properly representing vegetation dynamics in the future. Forest disturbances, resulting from heat and drought induced tree mortalities, wildfire, and insect outbreaks, are projected to increase in the future (Allen et al. 2010; McDowell et al. 2018; Williams et al. 2013; Anderegg et al. 2022) and forest disturbances can exacerbate projected decreases in streamflow, especially when combined with changes in climate (Bennett et al. 2018a).

Challenges also persist in model calibration and the fidelity of the meteorological datasets used to calibrate the model. For instance, snow albedo parameters are spatially consistent throughout the modeling domain and therefore VIC as currently implemented cannot account for the spatiotemporal variability of dust on snow in the basin (Deems et al. 2013; Painter et al. 2010, 2018), which is generally more prevalent in the San Juan Mountains than the northern Colorado Rockies. Additionally, at SNOTEL sites within the upper and lower Colorado River basin, the October through peak SWE precipitation totals from the Livneh et al. (2013) dataset were less than observed peak SWE at 28% of the SNOTEL sites suggesting that no changes to the model parameters would allow for SWE to be properly simulated. These two factors challenged model calibration against available SNOTEL data and the proper simulation of evapotranspiration and runoff, especially in many of the headwater locations.

Additional challenges persist regarding soil calibration. Our traditional individual catchment calibration approach resulted in a spatial patchwork of model parameters based on available streamflow gauges (Fig. S3). Parameter regionalization techniques such as the multiscale parameter regionalization (MPR; Samaniego et al. 2010) have been shown to provide a promising path forward to seamlessly estimate soil parameters over large domains (Gou et al. 2021; Rakovec et al. 2016, 2019; Samaniego et al. 2017). Mizukami et al. (2017) applied MPR to the VIC model for the CONUS-domain parameter estimation, showing deteriorated model performance in the Colorado River basin, relative to the other humid wet areas in CONUS. To improve streamflow simulations, further investigation of the MPR application to the VIC model (i.e., predictors, transfer functions, and scaling operators) is needed. In addition, the calibration strategy did not explicitly assess whether the optimized parameter sets could be as valid in future conditions as in historical ones. Calibrations that purposefully emphasize historically dry or wet periods might be more appropriate to provide realistic streamflow projections in a future climate, depending on projected conditions (Vaze et al. 2010). Further research into trend-response and parameter estimation strategies across all aspects of the modeling system is strongly recommended.

Last, we note that to explore the full range of streamflow projections, additional emissions scenarios, downscaling methods, hydrologic models, and the CMIP6 dataset should be explored (Samaniego et al. 2018, 2019; Vano et al. 2012, 2014). RCP8.5 was used here to represent a high emissions, high-risk scenario, that amplified the model's sensitivity relative to other emission scenarios (Hausfather and Peters 2020). Bias corrected and downscaled CMIP6 data, which can be used for hydrologic projections are forthcoming. Initial comparisons between CMIP5 and CMIP6 over western North America show similar precipitation and temperature changes in the ensemble mean (Li et al. 2021; Lukas and Payton 2020). However, more explicit, regional comparisons between CMIP5 and CMIP6 over the Colorado River basin should be explored. Therefore, these results suggest that policy makers should consider the sensitivity of the hydrologic projections to the vegetation decisions, but simultaneously understand that to determine the full range of future streamflow projections, additional emissions scenarios, hydrologic models, and climate scenarios should be explored.

5. Conclusions

We combined a recently published, updated vegetation dataset based on MODIS satellite imagery with a basin-by-basin calibration of VIC's soil parameters to produce a new VIC model configuration over the Colorado River basin. After calibration, the MODIS-informed VIC configuration showed similar streamflow performance to the previous VIC configuration used by decision makers to make informed climate change decisions about future water resources within the basin. Despite similar historic streamflow performance, the ensemble mean from the MODIS-based VIC configuration projected an end-of-century annual streamflow volume change of 0.4% at Lees Ferry, AZ, compared to the historical period (1960–2005). This projected change in streamflow is in contrast to prior ensemble mean projections that were used in recent climate impact studies that showed an 11.7% decline. Furthermore, the MODIS-based VIC configuration resulted in a greater spread in the projected changes of annual streamflow volume.

These results highlighted the need to accurately represent the vegetation characteristics and distribution in climate change studies, especially in arid environments. The MODIS-based parameters generally contained lower leaf area index values and also introduced fractional vegetation within each vegetated area of the grid cell. These new MODIS parameters resulted in evapotranspiration increases by the end of the century that were less than in the previous VIC configuration. Evapotranspiration differences were primarily in the upper basin's mountainous and forested areas, or in areas with high runoff ratios. Therefore, the differences in projected evapotranspiration caused substantial differences in end-of-century streamflow projections. These differences were primarily due to lower leaf area index values, the representation of fractional vegetation within the MODIS-based VIC tiles, and a general reduction in the forested area. The substantial difference in end-of-century streamflow projections signified the need to accurately represent evapotranspiration especially as temperatures increase and vegetation changes.

Acknowledgments. This research was made possible through the support of the Colorado River Climate and Hydrology Work Group and was funded by the U.S. Bureau of Reclamation, Central Arizona Water Conservation District, Denver Water, California's Six Agency Committee, Southern Nevada Water Authority, and the Wyoming State Engineer's Office. We gratefully acknowledge funding from Bureau Reclamation Grant 20190089 through AGS-1935447 NSF-GEO and Southern Nevada Water Authority, Grant 20190090. We also want to thank Joseph J. Barsugli and two anonymous reviewers for helpful comments and discussion on a previous version of this paper. Furthermore, we would like to acknowledge high-performance computing support from Cheyenne (doi:10.5065/D6RX99HX), provided by NCAR's Computational and Information Systems Laboratory, sponsored by the National Science Foundation. Additionally, we greatly benefited from the following open-source libraries to perform analyses presented in this study: numpy (Van Der Walt et al. 2011), pandas (McKinney 2010), geopandas (Jordahl et al. 2020), xarray (Hoyer and Hamman 2017), matplotlib (Hunter 2007), and cartopy (Met Office 2015). We acknowledge the World Climate Research Programme's Working Group on Coupled Modelling, which is responsible for CMIP, and we thank the climate and modeling groups (listed in Table S4 of the supplemental material) for producing and making available their model output. For CMIP the U.S. Department of Energy's Program for Climate Model Diagnosis and Intercomparison provides coordinating support and led development of software infrastructure in partnership with the Global Organization for Earth System Science Portals.

Data availability statement. Colorado River naturalized streamflow data are available here: https://www.usbr.gov/lc/region/g4000/NaturalFlow/documentation.html. LOCA data can be accessed from a number of locations outlined on this website: http://loca.ucsd.edu/. The LOCA-VIC runs identified as $VIC_{LOCA\text{-}L13}$ are archived here: https://gdo-dcp.ucllnl.org/downscaled_cmip_projections/#Welcome. The Bohn and Vivoni (2019) data can be found at https://doi.org/10.5281/zenodo.2559631. The Livneh et al. (2013) data can be found here: https://psl.noaa.gov/data/gridded/data.livneh.html. All other data are archived at https://doi.org/10.5281/zenodo.8118027.

REFERENCES

Addor, N., O. Rössler, N. Köplin, M. Huss, R. Weingartner, and J. Seibert, 2014: Robust changes and sources of uncertainty in the projected hydrological regimes of Swiss catchments. *Water Resour. Res.*, **50**, 7541–7562, https://doi.org/10.1002/2014WR015549.

Alder, J. R., and S. W. Hostetler, 2019: The dependence of hydroclimate projections in snow-dominated regions of the western United States on the choice of statistically downscaled climate data. *Water Resour. Res.*, **55**, 2279–2300, https://doi.org/10.1029/2018WR023458.

Allen, C. D., and Coauthors, 2010: A global overview of drought and heat-induced tree mortality reveals emerging climate change risks for forests. *For. Ecol. Manage.*, **259**, 660–684, https://doi.org/10.1016/j.foreco.2009.09.001.

Anderegg, W. R. L., and Coauthors, 2022: Future climate risks from stress, insects and fire across US forests. *Ecol. Lett.*, **25**, 1510–1520, https://doi.org/10.1111/ele.14018.

Andreadis, K. M., P. Storck, and D. P. Lettenmaier, 2009: Modeling snow accumulation and ablation processes in forested environments. *Water Resour. Res.*, **45**, W05429, https://doi.org/10.1029/2008WR007042.

Bastola, S., C. Murphy, and J. Sweeney, 2011: Evaluation of the transferability of hydrological model parameters for simulations under changed climatic conditions. *Hydrol. Earth Syst. Sci. Discuss.*, **8**, 5891–5915, https://doi.org/10.5194/hessd-8-5891-2011.

Beck, H. E., N. E. Zimmermann, T. R. McVicar, N. Vergopolan, A. Berg, and E. F. Wood, 2018: Present and future Köppen-Geiger climate classification maps at 1-km resolution. *Sci. Data*, **5**, 180214, https://doi.org/10.1038/sdata.2018.214.

Bennett, A. R., J. J. Hamman, and B. Nijssen, 2020: MetSim: A Python package for estimation and disaggregation of meteorological data. *J. Open Source Software*, **5**, 2042, https://doi.org/10.21105/joss.02042.

Bennett, K. E., T. J. Bohn, K. Solander, N. G. McDowell, C. Xu, E. Vivoni, and R. S. Middleton, 2018a: Climate-driven disturbances in the San Juan River sub-basin of the Colorado River. *Hydrol. Earth Syst. Sci.*, **22**, 709–725, https://doi.org/10.5194/hess-22-709-2018.

——, J. R. Urrego Blanco, A. Jonko, T. J. Bohn, A. L. Atchley, N. M. Urban, and R. S. Middleton, 2018b: Global sensitivity of simulated water balance indicators under future climate change in the Colorado basin. *Water Resour. Res.*, **54**, 132–149, https://doi.org/10.1002/2017WR020471.

Bohn, T. J., and E. R. Vivoni, 2016: Process-based characterization of evapotranspiration sources over the North American monsoon region. *Water Resour. Res.*, **52**, 358–384, https://doi.org/10.1002/2015WR017934.

——, and ——, 2019: MOD-LSP, MODIS-based parameters for hydrologic modeling of North American land cover change. *Sci. Data*, **6**, 144, https://doi.org/10.1038/s41597-019-0150-2.

——, B. Livneh, J. W. Oyler, S. W. Running, B. Nijssen, and D. P. Lettenmaier, 2013: Global evaluation of MTCLIM and related algorithms for forcing of ecological and hydrological models. *Agric. For. Meteor.*, **176**, 38–49, https://doi.org/10.1016/j.agrformet.2013.03.003.

Bosshard, T., M. Carambia, K. Goergen, S. Kotlarski, P. Krahe, M. Zappa, and C. Schär, 2013: Quantifying uncertainty sources in an ensemble of hydrological climate-impact projections. *Water Resour. Res.*, **49**, 1523–1536, https://doi.org/10.1029/2011WR011533.

Brekke, L., B. Thrasher, E. P. Maurer, and T. Pruitt, 2013: Downscaled CMIP3 and CMIP5 climate projections: Release of downscaled CMIP5 climate projections, comparison with preceding information, and summary of user needs. *Tech. Rep.*, 104 pp., https://gdo-dcp.ucllnl.org/downscaled_cmip_projections/techmemo/downscaled_climate.pdf.

——, A. Wood, and T. Pruitt, 2014: Downscaled CMIP3 and CMIP5 hydrology projections. Release of hydrology projections, comparison with preceding information, and summary of user needs. *Tech. Rep.*, 110 pp., https://gdo-dcp.ucllnl.org/downscaled_cmip_projections/techmemo/BCSD5HydrologyMemo.pdf.

Chegwidden, O. S., and Coauthors, 2019: How do modeling decisions affect the spread among hydrologic climate change projections? Exploring a large ensemble of simulations across a

diversity of hydroclimates. *Earth's Future*, **7**, 623–637, https://doi.org/10.1029/2018EF001047.

Chen, X., L. Vierling, D. Deering, and A. Conley, 2005: Monitoring boreal forest leaf area index across a Siberian burn chronosequence: A MODIS validation study. *Int. J. Remote Sens.*, **26**, 5433–5451, https://doi.org/10.1080/01431160500285142.

Christensen, N. S., and D. P. Lettenmaier, 2007: A multimodel ensemble approach to assessment of climate change impacts on the hydrology and water resources of the Colorado River basin. *Hydrol. Earth Syst. Sci.*, **11**, 1417–1434, https://doi.org/10.5194/hess-11-1417-2007.

——, A. W. Wood, N. Voisin, D. P. Lettenmaier, and R. N. Palmer, 2004: The effects of climate change on the hydrology and water resources of the Colorado River basin. *Climatic Change*, **62**, 337–363, https://doi.org/10.1023/B:CLIM.0000013684.13621.1f.

Daly, C., M. Halbleib, J. I. Smith, W. P. Gibson, M. K. Doggett, G. H. Taylor, J. Curtis, and P. P. Pasteris, 2008: Physiographically sensitive mapping of climatological temperature and precipitation across the conterminous United States. *Int. J. Climatol.*, **28**, 2031–2064, https://doi.org/10.1002/joc.1688.

Deems, J. S., T. H. Painter, and D. C. Finnegan, 2013: Lidar measurement of snow depth: A review. *J. Glaciol.*, **59**, 467–479, https://doi.org/10.3189/2013JoG12J154.

Falcone, J. A., 2011: GAGES-II: Geospatial attributes of gages for evaluating streamflow. U.S. Geological Survey, accessed 17 October 2020, https://doi.org/10.3133/70046617.

Ficklin, D. L., I. T. Stewart, and E. P. Maurer, 2013: Climate change impacts on streamflow and subbasin-scale hydrology in the upper Colorado River basin. *PLOS ONE*, **8**, e71297, https://doi.org/10.1371/journal.pone.0071297.

Gao, Y., J. A. Vano, C. Zhu, and D. P. Lettenmaier, 2011: Evaluating climate change over the Colorado River basin using regional climate models. *J. Geophys. Res.*, **116**, D13104, https://doi.org/10.1029/2010JD015278.

Gou, J., C. Miao, L. Samaniego, M. Xiao, J. Wu, and X. Guo, 2021: CNRD v1.0: A high-quality natural runoff dataset for hydrological and climate studies in China. *Bull. Amer. Meteor. Soc.*, **102**, E929–E947, https://doi.org/10.1175/BAMS-D-20-0094.1.

Gupta, H. V., H. Kling, K. K. Yilmaz, and G. F. Martinez, 2009: Decomposition of the mean squared error and NSE performance criteria: Implications for improving hydrological modelling. *J. Hydrol.*, **377**, 80–91, https://doi.org/10.1016/j.jhydrol.2009.08.003.

Hamman, J. J., B. Nijssen, T. J. Bohn, D. R. Gergel, and Y. Mao, 2018: The Variable Infiltration Capacity model version 5 (VIC-5): Infrastructure improvements for new applications and reproducibility. *Geosci. Model Dev.*, **11**, 3481–3496, https://doi.org/10.5194/gmd-11-3481-2018.

Hansen, M. C., R. S. Defries, J. R. G. Townshend, and R. Sohlberg, 2000: Global land cover classification at 1 km spatial resolution using a classification tree approach. *Int. J. Remote Sens.*, **21**, 1331–1364, https://doi.org/10.1080/014311600210209.

Harding, B. L., A. W. Wood, and J. R. Prairie, 2012: The implications of climate change scenario selection for future streamflow projection in the upper Colorado River basin. *Hydrol. Earth Syst. Sci.*, **16**, 3989–4007, https://doi.org/10.5194/hess-16-3989-2012.

Hausfather, Z., and G. P. Peters, 2020: Emissions - The "business as usual" story is misleading. *Nature*, **577**, 618–620, https://doi.org/10.1038/d41586-020-00177-3.

Hoerling, M., J. Barsugli, B. Livneh, J. Eischeid, X. Quan, and A. Badger, 2019: Causes for the century-long decline in Colorado River flow. *J. Climate*, **32**, 8181–8203, https://doi.org/10.1175/JCLI-D-19-0207.1.

Hoyer, S., and J. J. Hamman, 2017: xarray: N-D labeled arrays and datasets in python. *J. Open Res. Software*, **5**, 10, https://doi.org/10.5334/jors.148.

Hunter, J. D., 2007: Matplotlib: A 2D graphics environment. *Comput. Sci. Eng.*, **9**, 90–95, https://doi.org/10.1109/MCSE.2007.55.

Jensen, J. L. R., K. S. Humes, A. T. Hudak, L. A. Vierling, and E. Delmelle, 2011: Evaluation of the MODIS LAI product using independent lidar-derived LAI: A case study in mixed conifer forest. *Remote Sens. Environ.*, **115**, 3625–3639, https://doi.org/10.1016/j.rse.2011.08.023.

Jordahl, K., and Coauthors, 2020: geopandas/geopandas: v0.8.1. Zenodo, accessed 12 April 2020, https://doi.org/10.5281/zenodo.3946761.

Lehner, F., A. W. Wood, J. A. Vano, D. M. Lawrence, M. P. Clark, and J. S. Mankin, 2019: The potential to reduce uncertainty in regional runoff projections from climate models. *Nat. Climate Change*, **9**, 926–933, https://doi.org/10.1038/s41558-019-0639-x.

Li, D., M. L. Wrzesien, M. Durand, J. Adam, and D. P. Lettenmaier, 2017: How much runoff originates as snow in the western United States, and how will that change in the future? *Geophys. Res. Lett.*, **44**, 6163–6172, https://doi.org/10.1002/2017GL073551.

Li, J., R. Huo, H. Chen, Y. Zhao, and T. Zhao, 2021: Comparative assessment and future prediction using CMIP6 and CMIP5 for annual precipitation and extreme precipitation simulation. *Front. Earth Sci.*, **9**, 687976, https://doi.org/10.3389/feart.2021.687976.

Liang, X., D. P. Lettenmaier, E. F. Wood, and S. J. Burges, 1994: A simple hydrologically based model of land surface water and energy fluxes for general circulation models. *J. Geophys. Res.*, **99**, 14 415–14 428, https://doi.org/10.1029/94JD00483.

Lins, H. F., 2012: USGS Hydro-Climatic Data Network 2009 (HCDN-2009). USGS Fact Sheet 2012-3047, 4 pp., https://pubs.usgs.gov/fs/2012/3047/.

Livneh, B., E. A. Rosenberg, C. Lin, B. Nijssen, V. Mishra, K. M. Andreadis, E. P. Maurer, and D. P. Lettenmaier, 2013: A long-term hydrologically based dataset of land surface fluxes and states for the conterminous United States: Update and extensions. *J. Climate*, **26**, 9384–9392, https://doi.org/10.1175/JCLI-D-12-00508.1.

Lohmann, D., R. Nolte-Holube, and E. Raschke, 1996: A large-scale horizontal routing model to be coupled to land surface parametrization schemes. *Tellus*, **48A**, 708–721, https://doi.org/10.3402/tellusa.v48i5.12200.

Lukas, J., and E. Payton, 2020: Colorado River Basin Climate and Hydrology: State of the Science. Western Water Assessment, University of Colorado Boulder Tech. Rep., 520 pp., https://doi.org/10.25810/3hcv-w477.

Matott, L. S., B. Hymiak, C. Reslink, C. Baxter, and S. Aziz, 2013: Telescoping strategies for improved parameter estimation of environmental simulation models. *Comput. Geosci.*, **60**, 156–167, https://doi.org/10.1016/j.cageo.2013.07.023.

Maurer, E. P., A. W. Wood, J. C. Adam, D. P. Lettenmaier, and B. Nijssen, 2002: A long-term hydrologically based dataset of land surface fluxes and states for the conterminous United States. *J. Climate*, **15**, 3237–3251, https://doi.org/10.1175/1520-0442(2002)015<3237:ALTHBD>2.0.CO;2.

McCabe, G. J., and D. M. Wolock, 2007: Warming may create substantial water supply shortages in the Colorado River basin. *Geophys. Res. Lett.*, **34**, L22708, https://doi.org/10.1029/2007GL031764.

McDowell, N. G., S. T. Michaletz, K. E. Bennett, K. C. Solander, C. Xu, R. M. Maxwell, and R. S. Middleton, 2018: Predicting chronic climate-driven disturbances and their mitigation. *Trends Ecol. Evol.*, **33**, 15–27, https://doi.org/10.1016/j.tree.2017.10.002.

McKinney, W., 2010: Data structures for statistical computing in Python. *Proc. Ninth Python Sci. Conf.*, Austin, TX, SciPy, 56–61, https://doi.org/10.25080/Majora-92bf1922-00a.

Mendoza, P. A., and Coauthors, 2015: Effects of hydrologic model choice and calibration on the portrayal of climate change impacts. *J. Hydrometeor.*, **16**, 762–780, https://doi.org/10.1175/JHM-D-14-0104.1.

Merz, R., J. Parajka, and G. Blöschl, 2011: Time stability of catchment model parameters: Implications for climate impact analyses. *Water Resour. Res.*, **47**, W02531, https://doi.org/10.1029/2010WR009505.

Met Office, 2015: Cartopy: A cartographic python library with a matplotlib interface. Python package, https://scitools.org.uk/cartopy.

Miller, D. A., and R. A. White, 1998: A conterminous United States multilayer soil characteristics dataset for regional climate and hydrology modeling. *Earth Interact.*, **2**, https://doi.org/10.1175/1087-3562(1998)002<0002:CUSMS>2.0.CO;2.

Milly, P. C. D., and K. A. Dunne, 2020: Colorado River flow dwindles as warming-driven loss of reflective snow energizes evaporation. *Science*, **367**, 1252–1255, https://doi.org/10.1126/science.aay9187.

Mizukami, N., and Coauthors, 2016: MizuRoute version 1: A river network routing tool for a continental domain water resources applications. *Geosci. Model Dev.*, **9**, 2223–2238, https://doi.org/10.5194/gmd-9-2223-2016.

——, M. P. Clark, A. J. Newman, A. W. Wood, E. D. Gutmann, B. Nijssen, O. Rakovec, and L. Samaniego, 2017: Towards seamless large-domain parameter estimation for hydrologic models. *Water Resour. Res.*, **53**, 8020–8040, https://doi.org/10.1002/2017WR020401.

Newman, A., K. Sampson, M. Clark, A. Bock, R. J. Viger, and D. Blodgett, 2014: A large-sample watershed-scale hydrometeorological dataset for the contiguous USA. UCAR/NCAR, accessed 17 October 2020, https://doi.org/10.5065/D6MW2F4D.

Newman, A. J., and Coauthors, 2015: Development of a large-sample watershed-scale hydrometeorological data set for the contiguous USA: Data set characteristics and assessment of regional variability in hydrologic model performance. *Hydrol. Earth Syst. Sci.*, **19**, 209–223, https://doi.org/10.5194/hess-19-209-2015.

Painter, T. H., J. S. Deems, J. Belnap, A. F. Hamlet, C. C. Landry, and B. Udall, 2010: Response of Colorado River runoff to dust radiative forcing in snow. *Proc. Natl. Acad. Sci. USA*, **107**, 17 125–17 130, https://doi.org/10.1073/pnas.0913139107.

——, S. M. Skiles, J. S. Deems, W. T. Brandt, and J. Dozier, 2018: Variation in rising limb of Colorado River snowmelt runoff hydrograph controlled by dust radiative forcing in snow. *Geophys. Res. Lett.*, **45**, 797–808, https://doi.org/10.1002/2017GL075826.

Pierce, D. W., D. R. Cayan, and B. L. Thrasher, 2014: Statistical downscaling using localized constructed analogs (LOCA). *J. Hydrometeor.*, **15**, 2558–2585, https://doi.org/10.1175/JHM-D-14-0082.1.

——, ——, E. P. Maurer, J. T. Abatzoglou, and K. C. Hegewisch, 2015: Improved bias correction techniques for hydrological simulations of climate change. *J. Hydrometeor.*, **16**, 2421–2442, https://doi.org/10.1175/JHM-D-14-0236.1.

Prairie, J., and R. Callejo, 2005: Natural flow and salt computation methods, calendar years 1971–1995. U.S. Department of the Interior, Bureau of Reclamation, 112 pp.

Rakovec, O., and Coauthors, 2016: Multiscale and multivariate evaluation of water fluxes and states over European river basins. *J. Hydrometeor.*, **17**, 287–307, https://doi.org/10.1175/JHM-D-15-0054.1.

——, N. Mizukami, R. Kumar, A. J. Newman, S. Thober, A. W. Wood, M. P. Clark, and L. Samaniego, 2019: Diagnostic evaluation of large-domain hydrologic models calibrated across the contiguous United States. *J. Geophys. Res. Atmos.*, **124**, 13 991–14 007, https://doi.org/10.1029/2019JD030767.

Rumsey, C. A., M. P. Miller, D. D. Susong, F. D. Tillman, and D. W. Anning, 2015: Regional scale estimates of baseflow and factors influencing baseflow in the upper Colorado River basin. *J. Hydrol.*, **4**, 91–107, https://doi.org/10.1016/j.ejrh.2015.04.008.

Samaniego, L., R. Kumar, and S. Attinger, 2010: Multiscale parameter regionalization of a grid-based hydrologic model at the mesoscale. *Water Resour. Res.*, **46**, W05523, https://doi.org/10.1029/2008WR007327.

——, and Coauthors, 2017: Toward seamless hydrologic predictions across spatial scales. *Hydrol. Earth Syst. Sci.*, **21**, 4323–4346, https://doi.org/10.5194/hess-21-4323-2017.

——, and Coauthors, 2018: Anthropogenic warming exacerbates European soil moisture droughts. *Nat. Climate Change*, **8**, 421–426, https://doi.org/10.1038/s41558-018-0138-5.

——, and Coauthors, 2019: Hydrological forecasts and projections for improved decision-making in the water sector in Europe. *Bull. Amer. Meteor. Soc.*, **100**, 2451–2472, https://doi.org/10.1175/BAMS-D-17-0274.1.

Seager, R., and Coauthors, 2007: Model projections of an imminent transition to a more arid climate in southwestern North America. *Science*, **316**, 1181–1184, https://doi.org/10.1126/science.1139601.

——, M. Ting, C. Li, N. Naik, B. Cook, J. Nakamura, and H. Liu, 2013: Projections of declining surface-water availability for the southwestern United States. *Nat. Climate Change*, **3**, 482–486, https://doi.org/10.1038/nclimate1787.

Storck, P., 2000: Trees, snow and flooding: An investigation of forest canopy effects on snow accumulation and melt at the plot and watershed scales in the Pacific Northwest. Water Resources Series Tech. Rep. 161, University of Washington, 195 pp., https://www.ce.washington.edu/sites/cee/files/pdfs/research/hydrology/water-resources/WRS161.pdf.

Tian, Y., and Coauthors, 2004: Comparison of seasonal and spatial variations of leaf area index and fraction of absorbed photosynthetically active radiation from Moderate Resolution Imaging Spectroradiometer (MODIS) and Common Land Model. *J. Geophys. Res.*, **109**, D01103, https://doi.org/10.1029/2003JD003777.

Tolson, B. A., and C. A. Shoemaker, 2007: Dynamically dimensioned search algorithm for computationally efficient watershed model calibration. *Water Resour. Res.*, **43**, W01413, https://doi.org/10.1029/2005WR004723.

Udall, B., and J. Overpeck, 2017: The twenty-first century Colorado River hot drought and implications for the future. *Water Resour. Res.*, **53**, 2404–2418, https://doi.org/10.1002/2016WR019638.

U.S. Bureau of Reclamation, 2011a: West-Wide Climate Risk Assessments: Bias-corrected and spatially downscaled surface water projections. Tech. Memo. 86-68210-2011-01, 122 pp., https://www.usbr.gov/watersmart/docs/west-wide-climate-risk-assessments.pdf.

——, 2011b: Colorado River Basin Water Supply and Demand Study: Status Report. Interim Rep. 1, 69 pp., https://www.usbr.gov/lc/region/programs/crbstudy/Report1/StatusRpt.pdf.

——, 2012: Appendix C11 Modeling of Lower Basin Tributaries in the Colorado River Simulation System. 19 pp., https://www.usbr.gov/lc/region/programs/crbstudy/finalreport/Technical%20Report%20C%20-%20Water%20Demand%20Assessment/TR-C_Appendix11_FINAL.pdf.

——, 2021: Water reliability in the west - 2021 secure water act report. USBR Rep., 54 pp., https://www.usbr.gov/climate/secure/.

USGCRP, 2018: *Impacts, Risks, and Adaptation in the United States: The Fourth National Climate Assessment, Volume II*. D. R. Reidmiller et al., Eds., USGCRP, 1470 pp.

Van Der Walt, S., S. C. Colbert, and G. Varoquaux, 2011: The NumPy array: A structure for efficient numerical computation. *Comput. Sci. Eng.*, **13**, 22–30, https://doi.org/10.1109/MCSE.2011.37.

Vano, J. A., T. Das, and D. P. Lettenmaier, 2012: Hydrologic sensitivities of Colorado River runoff to changes in precipitation and temperature. *J. Hydrometeor.*, **13**, 932–949, https://doi.org/10.1175/JHM-D-11-069.1.

——, and Coauthors, 2014: Understanding uncertainties in future Colorado River streamflow. *Bull. Amer. Meteor. Soc.*, **95**, 59–78, https://doi.org/10.1175/BAMS-D-12-00228.1.

Vano, J., and Coauthors, 2020: Comparing downscaled LOCA and BCSD CMIP5 climate and hydrology projections - Release of Downscaled LOCA CMIP5 Hydrology. USBR Tech Memo., 96 pp., https://gdo-dcp.ucllnl.org/downscaled_cmip_projections/techmemo/LOCA_BCSD_hydrology_tech_memo.pdf.

Vaze, J., D. A. Post, F. H. S. Chiew, J. M. Perraud, N. R. Viney, and J. Teng, 2010: Climate non-stationarity—Validity of calibrated rainfall-runoff models for use in climate change studies. *J. Hydrol.*, **394**, 447–457, https://doi.org/10.1016/j.jhydrol.2010.09.018.

Viger, R. J., and A. Bock, 2014: GIS features of the Geospatial Fabric for National Hydrologic Modeling. USGS, accessed 17 October 2020, https://doi.org/10.5066/F7542KMD.

Whitney, K. M., and Coauthors, 2023: Spatial attribution of declining Colorado River streamflow under future warming. *J. Hydrol.*, **617**, 129125, https://doi.org/10.1016/j.jhydrol.2023.129125.

Williams, P. A., and Coauthors, 2013: Temperature as a potent driver of regional forest drought stress and tree mortality. *Nat. Climate Change*, **3**, 292–297, https://doi.org/10.1038/nclimate1693.

Wood, A. W., and D. P. Lettenmaier, 2006: A test bed for new seasonal hydrologic forecasting approaches in the western United States. *Bull. Amer. Meteor. Soc.*, **87**, 1699–1712, https://doi.org/10.1175/BAMS-87-12-1699.

——, L. R. Leung, V. Sridhar, and D. P. Lettenmaier, 2004: Hydrologic implications of dynamical and statistical approaches to downscaling climate model outputs. *Climatic Change*, **62**, 189–216, https://doi.org/10.1023/B:CLIM.0000013685.99609.9e.